TOXICOLOGICAL SCIENCES **126(2)**, 372–390 (2012)
doi:10.1093/toxsci/kfr345
Advance Access publication January 4, 2012

# Mechanism of Inhibition of the ATPase Domain of Human Topoisomerase IIα by 1,4-Benzoquinone, 1,2-Naphthoquinone, 1,4-Naphthoquinone, and 9,10-Phenanthroquinone

Deepak Gurbani,*,† Vandna Kukshal,‡ Julian Laubenthal,§ Ashutosh Kumar,¶ Alok Pandey,¶ Sarita Tripathi,‡ Ashish Arora,‡ Swatantra K. Jain,† Ravishankar Ramachandran,‡ Diana Anderson,§ and Alok Dhawan‖,[1]

*Systems Toxicology and Health Risk Assessment Group, CSIR-Indian Institute of Toxicology Research, Lucknow-226001, Uttar Pradesh, India; †Department of Biotechnology, Jamia Hamdard, New Delhi-110062, India; ‡Molecular and Structural Biology Division, CSIR-Central Drug Research Institute, Lucknow-226001, Uttar Pradesh, India; §Division of Medical Sciences, University of Bradford, Bradford, West Yorkshire BD7 1DP, United Kingdom; ¶Nanomaterial Toxicology Group, CSIR-Indian Institute of Toxicology Research, Lucknow-226001, Uttar Pradesh, India; and ‖Institute of Life Sciences, Ahmedabad University, Vastrapur, Ahmedabad - 380015, Gujarat, India

[1]To whom correspondence should be addressed. Fax: +91-522-2628227. E-mail: alok.dhawan@ahduni.edu.in.

Received July 5, 2011; accepted December 7, 2011

**The inhibition of human topoisomerase IIα (Hu-TopoIIα), a major enzyme involved in maintaining DNA topology, repair, and chromosome condensation/decondensation results in loss of genomic integrity. In the present study, the inhibition of ATPase domain of Hu-TopoIIα as a possible mechanism of genotoxicity of 1,4-benzoquinone (BQ), hydroquinone (HQ), naphthoquinone (1,2-NQ and 1,4-NQ), and 9,10-phenanthroquinone (9,10-PQ) was investigated. *In silico* modeling predicted that 1,4-BQ, 1,2-NQ, 1,4-NQ, and 9,10-PQ could interact with Ser-148, Ser-149, Asn-150, and Asn-91 residues of the ATPase domain of Hu-TopoIIα. Biochemical inhibition assays with the purified ATPase domain of Hu-TopoIIα revealed that 1,4-BQ is the most potent inhibitor followed by 1,4-NQ > 1,2-NQ > 9,10-PQ > HQ. Ligand-binding studies using isothermal titration calorimetry revealed that 1,4-BQ, HQ, 1,4-NQ, 1,2-NQ, and 9,10-PQ enter into four sequentially binding site models inside the domain. 1,4-BQ exhibited the strongest binding, followed by 1,4-NQ > 1,2-NQ > 9,10-PQ > HQ, as revealed by their average $K_d$ values. The cellular fate of such inhibition was further evidenced by an increase in the number of Hu-TopoIIα-DNA cleavage complexes in the human lung epithelial cells (BEAS-2B) using trapped in agarose DNA immunostaining (TARDIS) assay, which utilizes antibody specific for Hu-TopoIIα. Furthermore, the increase in γ-H2A.X levels quantitated by flow cytometry and visualized by immunofluorescence microscopy illustrated that accumulation of DNA double-strand breaks inside the cells can be attributed to the inhibition of Hu-TopoIIα. These findings collectively suggest that 1,4-BQ, 1,2-NQ, 1,4-NQ, and 9,10-PQ inhibit the ATPase domain and potentially result in Hu-TopoIIα-mediated clastogenic and leukemogenic events.**

*Key Words:* **quinones; human topoisomerase II alpha; *in silico* modeling; ATPase inhibition; BEAS-2B human lung cells; DNA double-strand breaks.**

Quinones are by-products of partial combustion of biomass and fossil fuels, petroleum products (especially diesel), polycyclic aromatic hydrocarbons, and polychlorinated biphenyls. Because these quinones are ubiquitous environmental pollutants, humans are increasingly getting exposed. This poses health risks, including cancer. The toxicity studies of environmentally occurring quinones, such as naphthoquinones (1,2-NQ and 1,4-NQ) and phenanthroquinones (9,10-PQ), have reported that these compounds are capable of causing mutations, DNA damage, chromosomal aberrations, and altered signal transduction pathways. These toxic effects have been attributed to their electrophilic and redox-cycling properties and have been linked to various cancers, including leukemias (Bolton *et al.*, 2000; Kepley *et al.*, 2003; Rodriguez *et al.*, 2008; Shinyashiki *et al.*, 2009; Sumi and Kumagai, 2007; Verma, 2006). Bolton *et al.* (2000) have reviewed the toxicity of quinones and have attributed their genotoxic, cytotoxic, immunotoxic, and carcinogenic potential to two major mechanisms: (1) formation of reactive oxygen species and (2) molecular targets including tubulin, topoisomerase II, histone, and DNA. However, other studies have revealed that inhibition of topoisomerase IIα is the primary cellular enzyme targeted by quinones (Baker *et al.*, 2001; Lindsey *et al.*, 2004). The leukemogenic properties of benzene have also been attributed to the accumulation of its major quinone metabolites, such as 1,4-benzoquinone (1,4-BQ) and hydroquinone (HQ), in the bone marrow and inhibition of human topoisomerase IIα (Hu-TopoIIα). Hu-TopoIIα is a major enzyme known to maintain DNA topology, repair, and chromosome condensation/decondensation (Baker *et al.*, 2001; Eastmond *et al.*, 2005).

The enzyme maintains DNA topology inside the cells by generating a transient double-strand break (DSB) in one segment of DNA, facilitating the passage of the other duplex

© The Author 2012. Published by Oxford University Press on behalf of the Society of Toxicology. All rights reserved.
For permissions, please email: journals.permissions@oup.com

Downloaded from https://academic.oup.com/toxsci/article/126/2/372/1687885 by Ahmedabad University user on 01 May 2025

DNA and relegating the break. Hydrolysis of ATP is required for efficient catalysis of the holoenzyme, which involves a series of coordinated conformational changes regulating its binding and dissociation. The complete catalytic cycle involves transport of the T-strand of DNA through the G-strand with concomitant hydrolysis of one ATP molecule bound to the homodimer leading to closed clamp formation (Mueller-Planitz and Herschlag, 2008). However, the fate of such closed clamp following inhibition of ATP hydrolysis has not yet been completely investigated. The topo II inhibitors are classified into two categories: topo II poisons (etoposide, teniposide, doxorubicin, and their analogs) and catalytic inhibitors (aclarubicin, merbarone, and bisdioxopiperazines ICRF 187 and ICRF 193). Quinones such as 1,4-benzoquinone, metabolites of polychlorinated biphenyls, and acetaminophen act as Hu-TopoIIα poisons (Lindsey *et al*., 2004; Srinivasan *et al*., 2002). Bender *et al*. (2007) have shown that 1,4-benzoquinone forms covalent adducts with Cys-392 and Cys-405 of Hu-TopoIIα outside the ATPase domain. However, a recent study by Mondrala and Eastmond (2010) has shown that 1,4-benzoquinone has the potential to inhibit the entire catalytic cycle of the enzyme at multiple points. It was also concluded that cleavage complexes (Hu-TopoIIα-DNA) formed due to inhibition by 1,4-benzoquinone are reversible using high salt or EDTA concentration. It could be argued that any covalent modification such as cross-linking of the N-terminal domains at this stage could then not be reversed, and therefore, further research is warranted.

*In silico* approaches involving molecular docking provide an indispensable tool for identifying possible molecular targets and their interactions. Previously, such molecular modeling has shown that salvicine, a diterpenoid quinone, binds to and interacts with Asn-150, Arg-152, Asn-163, and Gly-164 residues of the ATPase domain of Hu-TopoIIα, leading to its inhibition (Hu *et al*., 2006). However, cellular consequences, such as localization of quinone-stabilized Hu-TopoIIα complexes and resulting DNA DSBs, were not investigated. Recently, Li *et al*. (2010) have shown that emodin, an anthraquinone followed similar inhibition of Hu-TopoIIα resulting in an increase in the number of DNA DSBs causing chromosomal aberrations and micronucleus induction. It is an acceptable view that purified ATPase domains could be utilized for exploratory inhibitory studies similar to the holoenzymes. However, it should also be noted that purified domains exhibit reduced ATPase activities, which are otherwise stimulated by the presence of DNA (Hu *et al*., 2002). Nevertheless, quantitative insights could still be obtained in exploring the mode of inhibition. Our earlier study had revealed that quinone metabolites of benzene, such as 1,4-benzoquinone and hydroquinone, could interact with Ser-148, Ser-149, Asn-91, and Asn-150 residues of the ATP-binding site of this enzyme (Pandey *et al*., 2009). Therefore, in the present study, an attempt was made to investigate whether 1,4-BQ, 1,2-NQ, 1,4-NQ, and 9,10-PQ inhibit the ATPase domain of Hu-TopoIIα and result in genotoxic insult to the cells. This should help in elucidating the precise mechanisms of inhibition of the Hu-TopoIIα enzyme and understanding the associated clastogenic events.

## MATERIALS AND METHODS

### *Chemicals and Consumables*

1,4-benzoquinone, 1,2-naphthoquinone, 1,4-naphthoquinone, 9,10-phenanthroquinone, hydroquinone, etoposide (prepared as 100mM stock kept at −20°C), malachite green, polyvinyl alcohol, ammonium molybdate, bovine serum albumin (BSA), HCl, Tris-HCl, KCl, $MgCl_2$, dithiothreitol (DTT), adenosine 5′-triphosphate disodium salt (ATP), adenosine 5′-(β,γ-imido) triphosphate tetralithium salt hydrate (AMP-PNP), dimethyl sulfoxide (DMSO), ampicillin, kanamycin, chloramphenicol, tween-20, glycerol, 3-[4,5-dimethylthiazole-2-yl]-2,5-diphenyltetrazolium bromide (MTT) were purchased from Sigma-Aldrich Co. (St Louis, MO). RPMI-1640 media, PBS, were purchased from Invitrogen (Invitrogen, Ltd., Paisley, U.K.). 4′,6-diamidino-2-phenylindole, dihydrochloride (DAPI) VECTASHIELD mounting medium was purchased from Vector Laboratories, U.K. Ni sepharose high performance (HP), HiTrap heparin (HP), Q-Sepharose fast flow (QFF), SP sepharose, and superdex-75 10/300 hiload size exclusion columns were purchased from GE Healthcare Bio-Sciences AB (Uppsala, Sweden). Isopropylthiogalactoside (IPTG; Fermentas UAB, Vilnius, Lithuania), syringe filter (0.22 μm) and 10 kDa Amicon ultra (Millipore, Carrigtwohill, Co, Cork, Ireland), human topoisomerase IIα primary antibody (Ki-S1; Millipore, Temecula, CA), Cy3-AffiniPure Goat Anti-Mouse IgG, F(ab′)2 fragment-specific secondary antibody (Jackson ImmunoResearch Laboratories, Inc., West Grove, PA), and anti-phospho-H2A.X (Ser-139)-fluorescein isothiocyanate (FITC) conjugate (Millipore) primary antibody were used. All other chemicals used were of analytical grade and purchased from Sigma-Aldrich Co.

### *Cell Lines and Cell Culture*

BEAS-2B (human bronchial epithelial; American Type Culture Collection [ATCC] number: CRL-9609) cell lines were obtained from ATCC (Manassas). BEAS-2B was cultured in RPMI-1640 media containing 300 mg/l l-glutamine, 2 g/l sodium bicarbonate, and 10 ml/l antibiotic and antimycotic solution (GIBCO; Invitrogen, Auckland, NZ), supplemented with 10% heat inactivated fetal bovine serum (FBS) (GIBCO; Invitrogen). The cells were kept at 37°C in a humidified atmosphere in 5% $CO_2$ incubator.

### *Expression Vectors and Host*

*Escherichia coli* derivative strains Rosetta(DE3)pLysS and BL21(DE3) were procured from Novagen (CN Biosciences, Inc., Merck KGaA, Darmstadt, Germany). pSB23 and pRK793 vectors encoding tobacco etch virus (TEV) protease and ATPase domain of Hu-TopoIIα, respectively, were a gift by Prof. Gregory L. Verdine, Department of Chemistry & Chemical Biology, Harvard University, USA. Vector construct (pSB23) expresses a protein having N-terminal $His_6$-tag followed by a maltose-binding protein (MBP) and Hu-TopoIIα ATPase with a TEV protease cleavage site present in between (Wei *et al*. 2005).

### In Silico *Docking Studies for Ligand Interactions*

All the quinone molecules (1,4-BQ, 1,4-NQ, 1,2-NQ, and 9,10-PQ) were sketched and energy optimized using a Merck Molecular Force Field (MMFF) (Figs. 1A–E). Molecular docking studies for different quinones were carried out with Hu-TopoIIα-ATPase domain as using generalised rigid PLP-based docking (GRIP) docking method available in BioPredicta tools of VLife Molecular Design Suite 4.0 software. The human topoisomerase IIα enzyme (1ZXM, pdb code) dimer was co-crystallized with AMP/PNP (structural analog of ATP). Only chain A of the crystal (dimer) was used for docking studies. The protein monomer was optimized for geometry correction followed by energy optimization using MMFF. Residues near 8 Å of AMP-PNP were taken for active site identification. The placement of all quinone molecules in the active site of topoisomerase II was done using GRIP

Downloaded from https://academic.oup.com/toxsci/article/126/2/372/1687885 by Ahmedabad University user on 01 May 2025

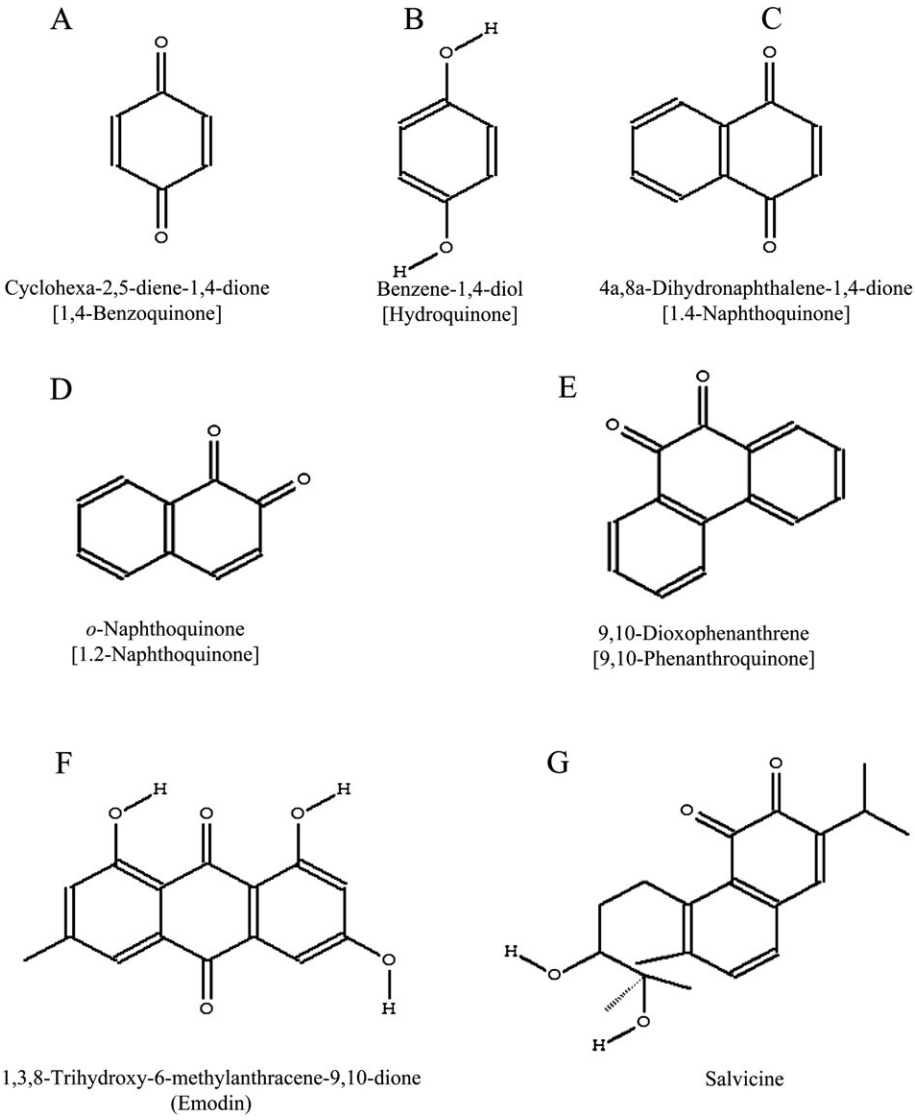



**FIG. 1.** Structures and names of the quinones used this study.

docking procedure and using cocrystal AMP/PNP ligand as a reference molecule. The method involved generating a grid around the reference ligand using piecewise linear pairwise (PLP) atom types, i.e., H-bond donor, H-bond acceptor, H-bond donor/acceptor, and nonpolar groups. All the molecules were positioned on the centroid of the grid based on lowest interaction energy grid points. Best docked conformations were analyzed by exploring the rotation of each quinone compound at 15° interval at the grid points and generated PLP score. A minimum PLP score describes the best aligned docked conformation in relation to the original cocrystallized ligand AMP-PNP. Finally, all the docked complexes were energy optimized, and $\Delta G$ (change in free energy on binding) was calculated as

$$\Delta G_{\text{binding}} = \Delta G_{\text{docked complex}} - [\Delta G_{\text{protein}} + \Delta G_{\text{ligand}}].$$

*Expression and Purification of ATPase Domain of Hu-TopoIIα*

Rosetta(DE3)pLysS cells were transformed with pSB23 vector. Seed culture was grown in Luria Bertani (LB; Hi Media Laboratories Pvt. Ltd., Mumbai, India) media at 37°C for overnight. Four liters LB media (supplemented with 35 μg/ml chloramphenicol and 50 μg/ml kanamycin) were inoculated with 1% seed culture and kept at 37°C/160 rpm. At $A_{600} \sim 0.8$, IPTG was added to final concentration of 1mM and further incubated for 12 h at 28°C/140 rpm. Expression was checked on 10% SDS-polyacrylamide gel electrophoresis (PAGE). Cells were harvested by centrifugation at 17,000 × g for 10 min at 4°C and resuspended in buffer-A (50mM Tris-HCl pH 7.0, 200mM NaCl, 10% glycerol) containing 10mM imidazole and protease inhibitor cocktail. The cells were then lysed by sonication (7 s on/6 s off, 40 cycles) on ice and centrifuged at 30,000 × g for 30 min at 4°C to remove the cell debris. The clear supernatant was then loaded onto a Ni-Sepharose HP column preequilibrated with buffer-A containing 10mM imidazole. Fusion protein ($His_6$-MBP-ATPase) was eluted with buffer-A containing 500mM imidazole. Eluted fractions were then dialyzed with buffer-B (50mM Tris-HCl pH 7.0, 5 mm EDTA, 2mM DTT, 10% glycerol) containing 50mM NaCl. Protein was further purified through heparin column and eluted with buffer-B containing 400mM NaCl. $His_6$-MBP-ATPase was then digested with TEV protease (1:100 protein) at 4°C for 12 h. The digested fractions were further dialyzed with buffer-B containing 50mM NaCl. $His_6$-MBP (47.2 kDa, pI 5.2) and ATPase domain (46 kDa, pI 8.93) were separated using QFF column preequilibrated with buffer-B containing 50mM

Downloaded from https://academic.oup.com/toxsci/article/126/2/372/1687885 by Ahmedabad University user on 01 May 2025

NaCl. Protein was eluted in flow-through fractions. Protein was further purified with a S-75 size exclusion column in buffer containing 100mM Tris-HCl (pH 7.4), 20mM KCl, 1mM DTT, 6mM $MgCl_2$, and 10% glycerol (Figs. 1A–D). Prior to biochemical experiments, the protein was dialyzed in assay buffer containing 100mM Tris-HCl, pH 7.4; 20mM KCl; 6mM $MgCl_2$ to remove DTT. Protein was concentrated with 10 kDa Centricon and concentration was estimated by Bradford's method (Bradford, 1976).

*Purification of TEV Protease*

BL21(DE3) was used as expression host for purification of TEV protease. Competent cells were transformed with pRK793 vector. One liter LB media (supplemented with 100 μg/ml ampicillin) was inoculated with 1% seed culture kept at 37°C. At $A_{600}$ ~ 0.4, IPTG was added to final concentration of 0.1mM and further incubated for 12 h at 22°C/120 rpm. Expression was checked on 10% SDS-PAGE. A single-step purification of TEV protease from a Ni-Sepharose column was done as described above and stored as 50% glycerol stock at −20°C.

*Confirmation of the Purified ATPase Domain of Hu-TopoIIα*

***Preparation of the protein sample.*** The protein band in the gel corresponding to 46 kDa in 10% SDS-PAGE, was excised, washed with Milli-Q (de-ionized) water, and kept twice for 10 min each with vortexing in destaining solution (15mM potassium ferricyanide, 50mM sodium thiosulphate). After repeated washing for 15 min, it was then incubated for 5 min with 100 μl of a solution containing 10mM ammonium bicarbonate and 50% acetonitrile. The proteins were reduced with 150 μl of 10mM DTT, 100mM ammonium bicarbonate, 5% acetonitrile for 1 h at 55°C, followed by dehydration of the gel band in 100 μl of 100% acetonitrile for 20 min. The proteins were further alkylated with 100 μl of 50mM iodoacetamide in 100mM ammonium bicarbonate for 30 min at room temperature in the dark. The gel band was then washed with 100 μl of 100mM ammonium bicarbonate for 10 min, followed by 100 μl of 100% acetonitrile for 20 min. The liquid was removed, and the gel band was dried in a SpeedVac for 15 min. The proteins in gel band were then digested with 150–200 ng trypsin in 50mM ammonium bicarbonate for 16 h at 37°C. The gel band was further treated once with 100 μl of 20mM ammonium bicarbonate, twice with 100 μl of 1% trifluoroacetic acid (TFA) in 50% acetonitrile for 20 min, and finally once again with 100 μl of 100% acetonitrile for 20 min. The extracted peptides were collected in the supernatant, pooled together, and concentrated in a SpeedVac to 10 μl.

***Mass spectrometry protein identification method (MALDI-TOF-TOF).*** From 10 μl of extracted peptides, 1 μl of the sample was mixed with 1 μl of α-cyano-4-hydroxycinnamic acid (5 mg/ml in 50% acetonitrile, 0.1% TFA; Bruker Daltonics) matrix and analyzed on a Bruker Ultraflex MALDI-TOF-TOF mass spectrometer with Flex Control v2.2 and processed using Flex analysis v2.2 software.

The standard peptide mixture (a mixture of nine peptides from the *m*/*z* range of 757–3147) was used for external mass calibration. Spectra were acquired for the mass-to-charge (*m*/*z*) range of 800–4000. All samples were analyzed in reflectron mode at laser power of 20–25%. Each spectrum was the sum of 500 laser shots with laser frequency of 50 Hz. The peak lists for mass spectrometry (MS) were generated using Flex control version 2.2 and Flex analysis version 2.2 (Bruker Daltonics). The peptide mass list was searched against the MSDB database using the MASCOT search engine (Bio Tools v2.2 software). The search parameters were set as follows: Database—MASCOT; enzyme—trypsin; taxonomy—Homo sapiens; global modification of carbamidomethyl on cysteine; with variable modification of oxidation on methionine; no restrictions on protein mass; and allowed up to one missed cleavage. The peptide tolerance was set at 100 ppm. For protein mass fingerprinting, only those proteins with score > 60 ($p < 0.05$) were accepted.

***Liquid chromatography-MS/MS analysis of the peptide ions.*** For MS-MS identification of peptides, a 6 μl solution of extracted peptides was injected into a liquid chromatography (LC)-MS/MS system (Agilent, Palo Alto, CA). This nLC system (Agilent 1100 NanoLC-1100 system) is combined with a microwell-plate sampler and thermostatted column compartment for preconcentration (LC Packings, Agilent). The samples were loaded on the column (Zorbax 300SB-C18, 150 mm × 75 μm, 3.5 μm) using a preconcentration step in a micro precolumn cartridge (Zorbax 300SB-C18, 5 mm × 300 μm, 5 μm). Six microliters of the sample was loaded on the precolumn at a 5 μl/min flow rate. After 5 min, the precolumn was connected with the separating column, and multistep gradient (3% until 5 min, 15% for 5–8 min, 45% for 8–50 min, 90% for 50–55 min, 90% for 55–70 min, then again 3% for 71 min) was started. The buffers used were (1) 0.1% HCOOH in water and (2) 0.1% HCOOH in 90% acetonitrile. An LC/MSD Trap XCT with a nanoelectrospray interface (Agilent) operated in the positive ion mode was used for MS. Ionization (1.5 kV ionization potential) was performed with a liquid junction and a noncoated capillary probe (New Objective, Cambridge). Calibration of the instrument was performed using the standard Agilent tuning mix. Peptide ions were analyzed by a full MS scan using the data-dependent method. The scan sequence consisted of single full MS scan followed by four MS/MS scans of the most abundant ions. Data were analyzed using Agilent Ion Trap Analysis software version 5.2, and proteins were identified by using MASCOT search tool against MASCOT database (www.matrixscience.com).

The experiments on Matrix Assisted Laser Desorption Ionization - Time of Flight (MALDI-TOF-TOF) and LC-MS/MS were performed at The Centre for Genomic Application, New Delhi.

*ATPase Domain–Related Assays*

***Determination of ATPase activity.*** The ATPase activity was measured using a nonisotopic malachite green assay (Rowlands *et al*., 2004). Briefly, a reagent containing malachite green (0.0812%, wt/vol), polyvinyl alcohol (2.32%, wt/vol), ammonium molybdate (5.72%, wt/vol, in 6M HCl), and Milli-Q water mixed in the ratio 2:1:1:2 was freshly prepared and kept at 4°C. A 100mM ATP stock solution was freshly prepared in the assay buffer containing 100mM Tris-HCl pH 7.4, 20mM KCl, and 6mM $MgCl_2$. A typical 100 μl reaction volume for measuring specific ATPase activity contained different concentrations of protein and substrate (ATP) and was incubated for different time points. Optimum protein concentration was obtained from the ATP hydrolysis assay and used for further studying the enzyme kinetics. Reactions were started by the addition of 250μM ATP and incubated for 2 h at 37°C. The reaction was terminated by the addition of 800 μl of malachite green reagent, and the absorbance was recorded at 620 nm on a microtiter plate reader (Synergy HT; BioTek). The optical density ($OD_{620}$) values obtained at each respective ATP concentration without enzyme were subtracted for background correction, and release of inorganic phosphate was calculated from a standard phosphate curve. For enzyme kinetics studies, reactions were carried out in triplicate as described above. The rate of enzyme reaction was analyzed using a nonlinear regression fit to the Michaelis-Menten equation. $K_m$ and $V_{max}$ values were obtained using linear regression analysis performed on double reciprocal plots (Lineweaver-Burk linear transformation) with rate of ATP hydrolysis versus ATP concentration (1/V vs. 1/S).

***Inhibition assays with the Hu-TopoIIα-ATPase domain.*** Inhibition of the ATPase activity described above was measured by adding different concentrations of quinones (dissolved in dimethyl sulfoxide [DMSO] [except hydroquinone], final concentration < 0.1%). Hydroquinone was dissolved in Milli-Q (deionized) water. The concentrations used were based on the relative potency of each compound, and $IC_{50}$ values were determined. To identify the mode of inhibition, 1,4-benzoquinone was added to the enzyme at different concentrations near $IC_{50}$ values against varying substrate (ATP) concentrations. To calculate $K_m^{app}$ and $V_{max}^{app}$, kinetic data for ATP hydrolysis were analyzed using linear regression analysis. Double reciprocal plot (Lineweaver-Burk linear transformation [1/V vs. 1/S]) for increasing inhibitor concentrations against ATP hydrolysis was interpolated to identify the intercepts for elucidating the correct mode of inhibition.

***Determination of binding constants of different quinones by isothermal titration calorimetry.*** Isothermal Titration Calorimetry (ITC) experiments were performed on a Microcal VP-ITC microcalorimeter (Northampton, MA) calibrated as per standard protocol. Reference cell was filled with Milli-Q. All

Downloaded from https://academic.oup.com/toxsci/article/126/2/372/1687885 by Ahmedabad University user on 01 May 2025

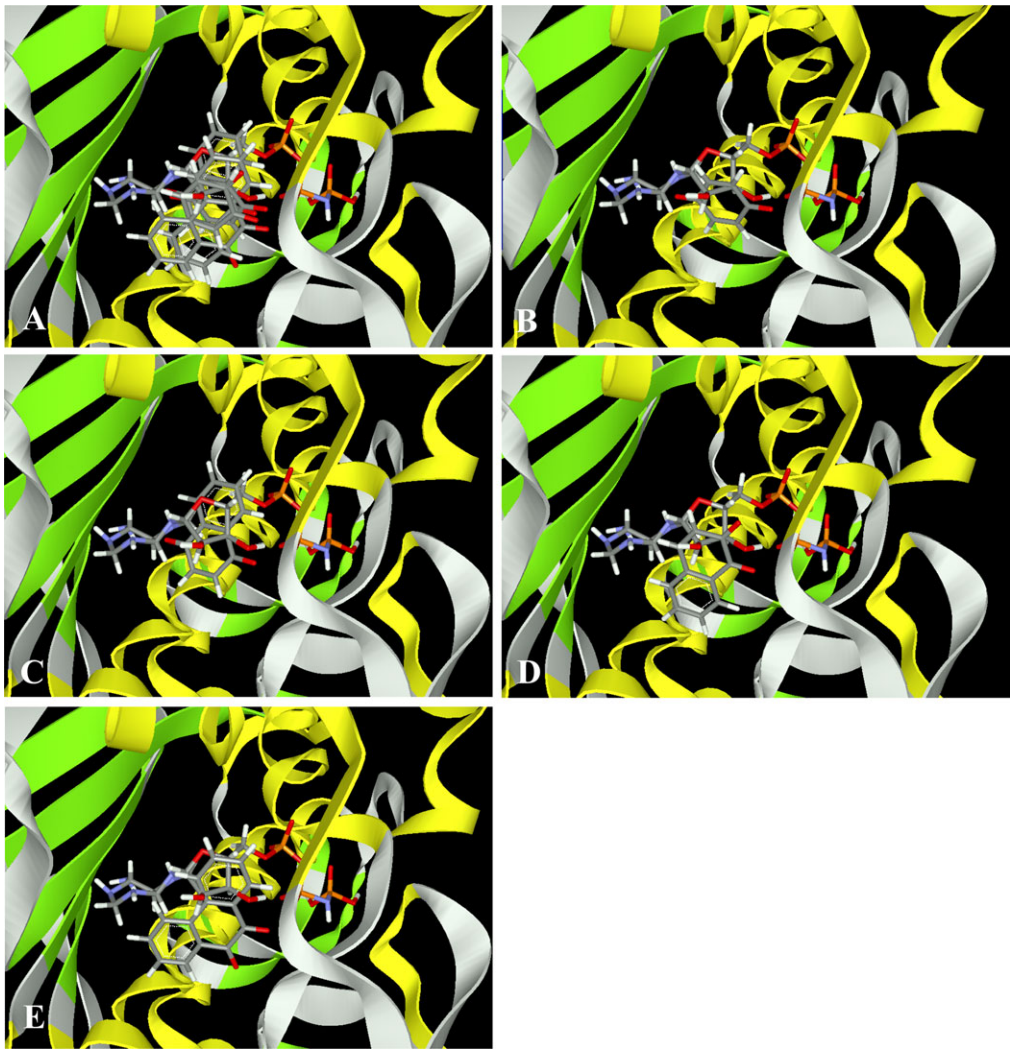



**FIG. 2.** Ribbon structures showing comparative molecular docking for quinones overlapped with adenosine 5′-(β,γ-imido) triphosphate (AMP-PNP) at the ATPase domain of Hu-TopoIIα. (A) Ribbon diagram showing all compounds placed together in the active site. The overlapping region near ribose ring of AMP-PNP is shown in each individual docked conformation for (B) 1,4-benzoquinone (C) 1,4-naphthoquinone, (D) 1,2-naphthoquinone, and (E) 9,10-phenanthroquinone. α-Helices are shown in yellow, β-sheets in green, and random coils in gray. All the molecules are depicted in stick, carbon, gray; nitrogen, blue; oxygen, red; hydrogen, white; and phosphorus, orange.

the ITC experiments were conducted in buffer containing 100mM Tris-HCl (pH 7.4), 20mM KCl, and 6mM $MgCl_2$. In each experiment, 1 μl of the respective ligand (quinone) solutions (100mM compound stock in DMSO) was added to 1 ml of buffer. A matched quantity of DMSO was added to the protein sample immediately prior to the experiment. The sample was then vortexed and centrifuged. All solutions were degassed for 10–15 min at 25°C prior to loading the samples in the ITC syringe and cell. All titrations were carried out at 30°C with a stirring speed of 416 rpm and duration of 240 s between each 10 μl injection. The titrant solution contained the ligand (0.1mM, 282 μl), and the reaction cell contained Hu-TopoIIα-ATPase domain (0.005mM, 1.44 mL). To correct the heats of dilution, control experiments were performed by making identical injections of the titrant solution into a cell containing only buffer with equal percentage of DMSO. These values were then subtracted from their respective titration prior to data analysis. The fitting of ITC data to different binding models by nonlinear least-squares approach (Levenberg-Marquardt algorithm) was done with Microcal Origin software package provided with the instrument. Thermal titration data were fitted to one or more of the three association models: "single set of identical sites," "two sets of independent sites," and "sequential binding sites." The models were compared by visual inspection of the fitted curves and by comparing the $\chi^2$ values obtained after the computation. The model resulting in the lowest value of $\chi^2$ was therefore considered as the best model to describe the molecular mechanism of binding. A sequential binding model provided a better fit to the data, and analysis yielded thermodynamic parameters association constant ($K_a$) and enthalpy of binding ($\Delta H$). Duplicate titrations were performed for each sample set to evaluate reproducibility. Average binding constants ($K_d$ values) were calculated as follows: $K_d = 1/(K1K2K3K4)^{1/4}$.

*Cellular Localization of Hu-TopoIIα-Quinone Complexes*

***Cytotoxicity assessment using MTT assay for assessment of mitochondrial succinate dehydrogenase activity.*** The MTT assay measures a decrease in mitochondrial succinate dehydrogenase activity, which in turn reflects live cells undergoing oxidative stress. Mitochondrial succinate dehydrogenase activity was assessed as described earlier (Mosmann, 1983). Briefly, BEAS-2B cells were seeded in 96-well plate in triplicate (density of $0.5 \times 10^5$ cells/ml in a final volume of 0.2 ml/well). Prior to treatment, the growth media were

Downloaded from https://academic.oup.com/toxsci/article/126/2/372/1687885 by Ahmedabad University user on 01 May 2025

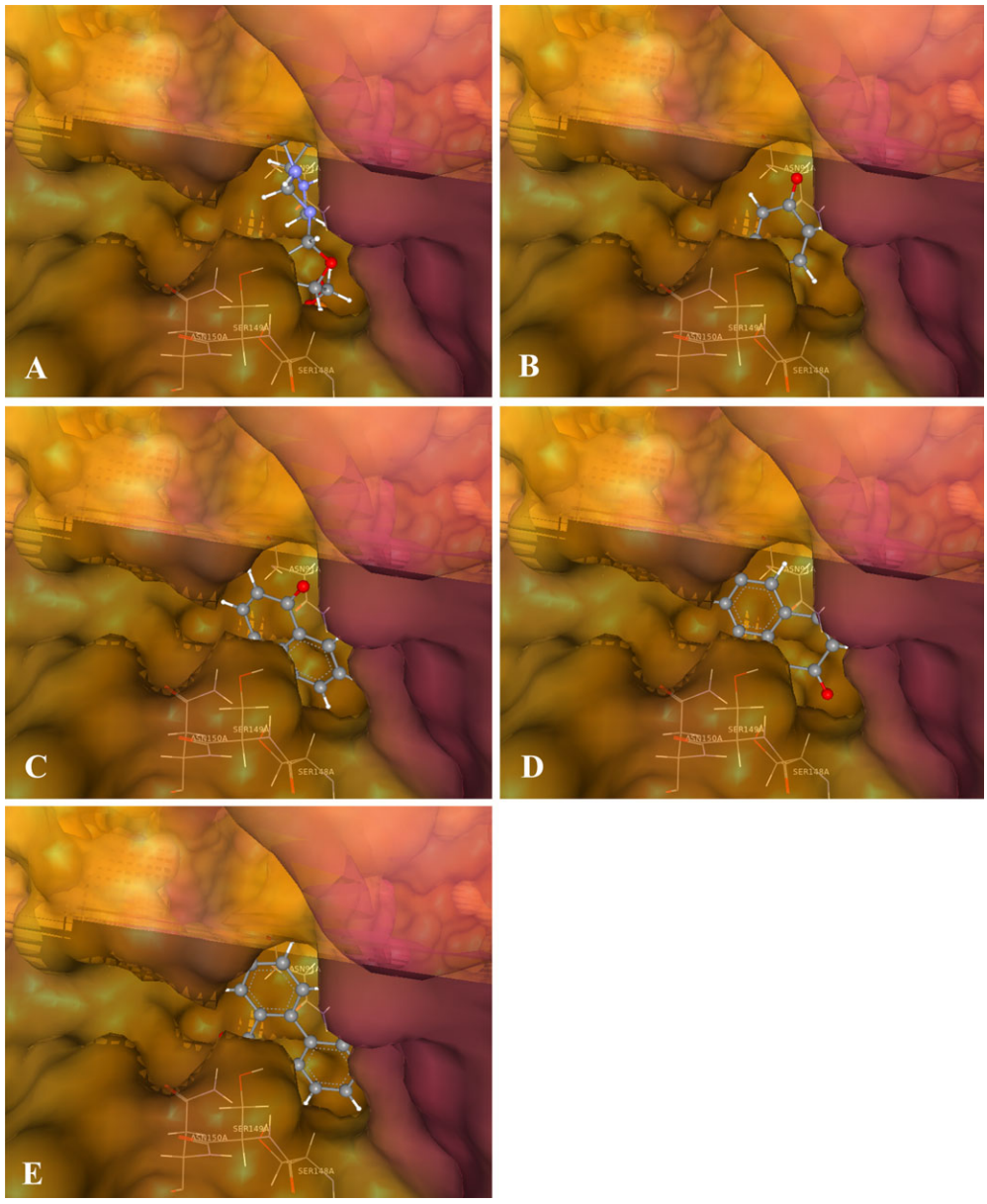



**FIG. 3.** Three-dimensional characterization of 46 kDa ATPase domain of Hu-TopoIIα mapped using electrostatic potential of the active site. View of modeled complexes showing placement for (A) adenosine 5′-(β,γ-imido) triphosphate, (B) 1,4-benzoquinone, (C) 1,4-naphthoquinone, (D) 1,2-naphthoquinone, and (E) 9,10-phenanthroquinone inside the cavity. Critical residues near the interaction site Ser-148, Ser-149, Asn-150, and Asn-91 are also shown.

removed and different concentrations (1–100μM) of all six quinone compounds prepared in incomplete RPMI-1640 (without FBS) media were added for 1 h. The treatment was removed, and MTT dye was added for a 4 h incubation period at 37°C. After this incubation period, the medium from each well was discarded and the resulting colored formazan crystals produced from MTT were dissolved in 200 μl of DMSO and absorbance at 530 nm was measured using multiwell plate reader (Synergy HT, BioTek) using KC4 software.

***Propidium iodide staining for quantification of dead cells.*** Propidium Iodide (PI) uptake assay discriminates between live/dead cell populations, and therefore, necrotic population (dead cells) is shown in the graph. PI is a fluorescent nucleic acid dye, which enters into the cells with the low membrane integrity. Loss of membrane integrity is a main characteristic of necrotic process. PI uptake assay is well suited for a high-throughput quantitation of dead cells in various cell culture assays using flow cytometry (O'Brien and Bolton, 1995). Therefore, BEAS-2B cells were treated with different concentrations (1–100μM) of all six quinone compounds as described above and harvested. Cells were washed twice with PBS and incubated with 1 μg/ml PI in PBS for 10 min at room temperature. Cytotoxicity assessment of BEAS-2B cells treated with quinones was done with each sample, and 10,000 cells were acquired using a flow cytometer (FACSCanto II; BD Biosciences, San Jose, CA) and analyzed by FACSDiva software Ver 6.1.2 (BD Biosciences).

***Detection and quantitation of quinone-stabilized Hu-TopoIIα-DNA complexes.*** Quinone-stabilized Hu-TopoIIα-DNA complexes were visualized in BEAS-2B cells using trapped in agarose DNA immunostaining (TARDIS) assay involving isoenzyme selective immunofluorescence microscopy

Downloaded from https://academic.oup.com/toxsci/article/126/2/372/1687885 by Ahmedabad University user on 01 May 2025

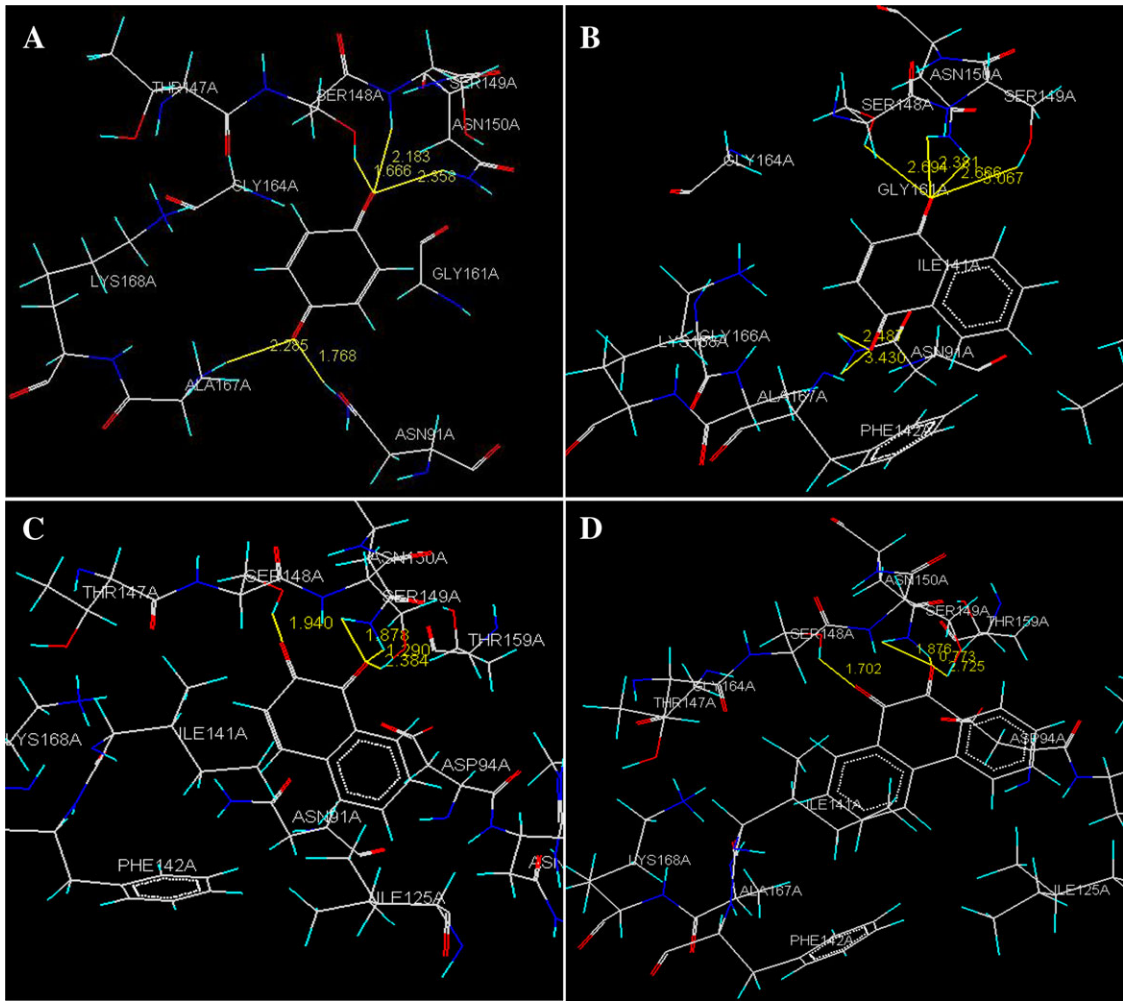



**FIG. 4.** Hydrogen-bonding interactions with the active site residues for (A) 1,4-benzoquinone, (B) 1,4-naphthoquinone, (C) 1,2-naphthoquinone, and (D) 9,10-phenanthroquinone inside the ATPase domain of Hu-TopoIIα.

(Willmore *et al*., 1998) with minor modifications. Briefly, BEAS-2B cells were treated with 1μM of BQ, 1,4-NQ, 1,2-NQ, 9,10-PQ, and HQ for 1 h. Etoposide (Et) was used as positive control at 1μM for same duration. Fifty microliters of cell suspension (~10,000 cells) was immediately mixed with an equal volume of low melting point agarose solution (2% wt/vol in PBS) warmed to 37°C. The mixture was spread evenly across a slide, and the agarose was quickly gelled by placing the slides on ice blocks. The slides were then immersed in lysis buffer (1% [wt/v] SDS, 80mM phosphate buffer, pH 6.8, 10mM EDTA, and a protease inhibitor mixture [2 mg/ml pepstatin A, 2 mg/ml leupeptin, 1mM phenylmethylsulfonyl fluoride, 1mM benzamidine, and 1mM DTT, final concentrations]) for 20 min at 20°C. DNA and Hu-TopoIIα-DNA complexes remained trapped in agarose. Slides were immersed in 1M NaCl supplemented with the protease inhibitor mixture for 1 h at 20°C to wash out free enzyme and further washed by immersion three times (15 min per wash) in PBS. Slides were then exposed to primary antibody Ki-S1 (1:100, diluted in PBS containing 0.1% [vol/vol] Tween 20 and 1% [wt/vol] BSA) for 1 h in a humidified atmosphere and washed three times in PBS containing 0.1% (vol/vol) Tween 20 (PBST). Because topoisomerase IIα antigen is preferentially expressed in actively dividing cells during G1, S, G2, and M phase of the cell cycle. Nondividing cells (i.e., G0 phase) lacks this enzyme. Therefore, constantly proliferating cells (e.g., cell lines used *in vitro*) react specifically to topoisomerase IIα during the entire cell cycle. The Ki-S1 antibody used recognizes a carboxy terminal a-isoenzyme-specific epitope missing in topoisomerase IIβ and therefore enables it to be used as marker for detection of the enzyme (Boege *et al*., 1995). Slides were further exposed to the cy3-conjugated goat anti-mouse secondary antibody recognizing IgG, $F(ab)_2$ of mouse (1:200, diluted in PBS containing 0.1% [vol/vol] Tween 20 and 1% [wt/vol] BSA) for 1 h before two washes in PBST and one final wash (30 min) in PBS containing the protease inhibitor mixture. DNA was visualized using DAPI (4,6′-diamidino-2-phenylindole) staining, and images were taken using epifluorescence microscope (Nikon 80i; Nikon Corporation, Japan).

The quantitative fluorescence image analysis of Hu-TopoIIα-DNA complexes was done using Leica AF lite software 2.1.0 build 4316 (Leica Microsystems CMS GmbH). The images were prior corrected for background using standard procedures before fluorescent measurements. Corrected images for blue (due to DAPI staining) and red fluorescence (due to Cy3-antibody staining) were used to identify the nuclear DNA and Hu-TopoIIα-DNA complexes.

### *DNA DSB Assessment*

***Quantitative γ-H2A.X determination by flow cytometry.*** γ-H2A.X, which is a marker of DNA DSBs, was assessed in the BEAS-2B cells as described earlier (Muslimovic *et al*., 2008). Briefly, $10^5$ cells were treated with different concentrations of quinones (0.1–10μM) at 37°C for 30 min in a $CO_2$ incubator. Treated cells were washed with PBS and harvested using trypsin. Cells were centrifuged at 3700 × g for 4 min at 4°C, and pellets were washed with ice cold

Downloaded from https://academic.oup.com/toxsci/article/126/2/372/1687885 by Ahmedabad University user on 01 May 2025

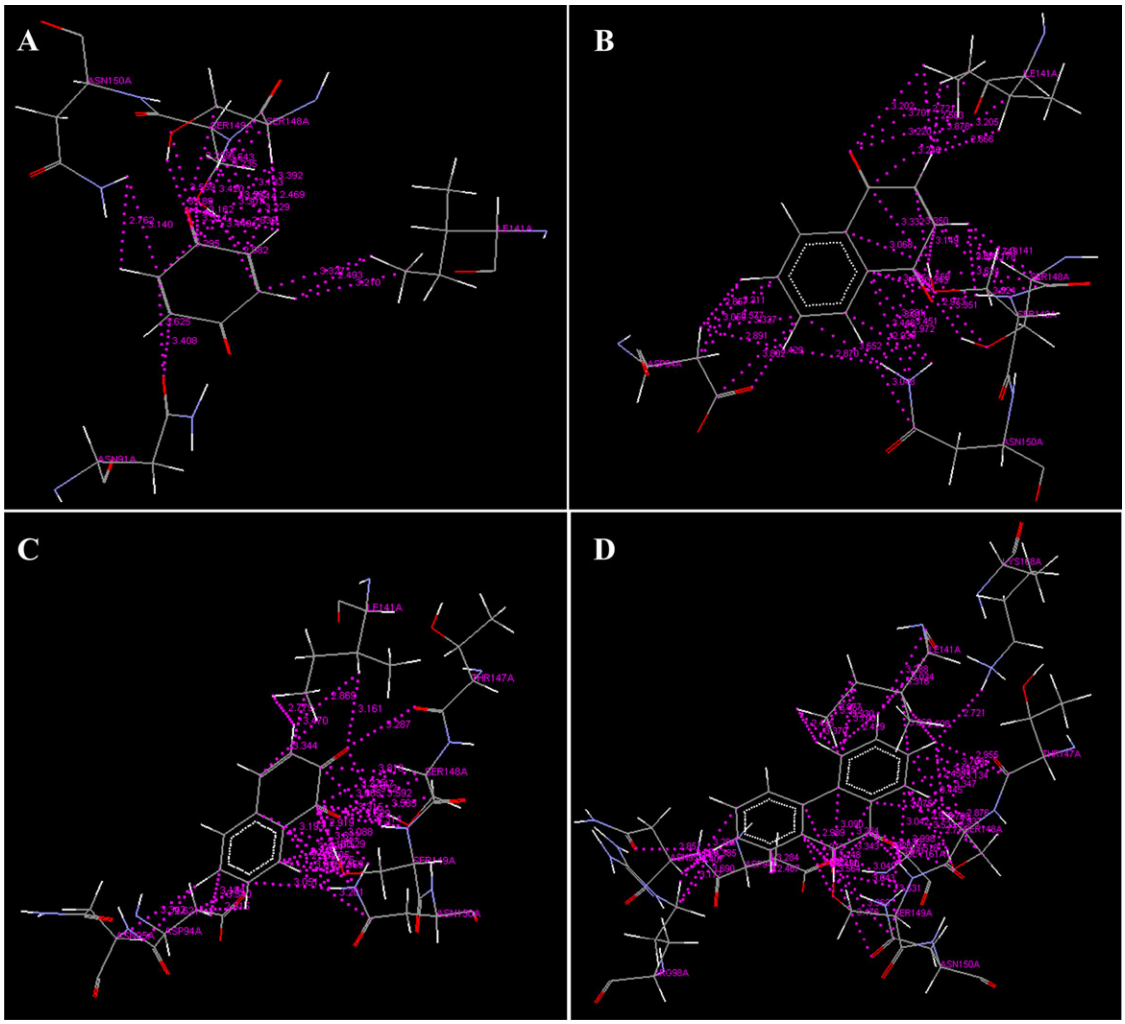



**FIG. 5.** Active-site residues conferring van der Waals interactions with (A) 1,4-benzoquinone, (B) 1,4-naphthoquinone, (C) 1,2-naphthoquinone, and (D) 9,10-phenanthroquinone inside the ATPase domain of Hu-TopoIIα.

PBS. After washing, pellets were resuspended in 150 µl of block 9 solution (PBS supplemented with 0.1% BSA, 8% FBS, 0.1 g/l RNaseA, 0.25 g/l herring sperm DNA, 0.1% triton X-100, 5mM EDTA, phosphatase inhibitors, and 0.1 g/ml sodium azide) with anti-phospho-H2A.X (Ser 139)-FITC conjugated antibody at a final concentration of 1 µg/ml. These samples were further incubated for 2.5 h at 4°C in the dark. After the incubation, samples were diluted in 350 µl of suspension buffer (0.1% BSA) and analyzed by flow cytometry using a 488 nm laser.

***Immunocytochemical detection of γ-H2A.X.*** BEAS-2B cells (10,000 cells/well) were seeded in a four-chamber glass slide and after 24 h, washed twice with 0.5 ml PBS and fixed by adding 0.5 ml of 4% PFA following incubation for 15 min. The cells were then washed thrice with 0.5 ml PBST (0.05% [vol/vol] Tween-20 in PBS) and further incubated for 30 min in 0.5 ml of 1% BSA. Cells were then washed with PBST (three times) and incubated in 0.2 ml of anti-phospho-histone H2A.X (Ser-139)-FITC conjugate antibody (about 1:100), diluted in 0.1% BSA, for 1 h at room temperature. Unbound antibody was washed out with 0.5 ml PBST. The chambered slide was opened and 15 µl of DAPI was added to each well and cover slip was placed. The images were captured using fluorescence microscope (Nikon Eclipse 80i equipped with Nikon DS-Ri1 camera) and merged using image analysis software Leica Qwin 500.

## RESULTS

### *In Silico* Docking Studies of Quinones

To identify the binding site interactions of different quinone pollutants inside the Hu-TopoIIα ATPase domain, different docked conformations for each quinone were analyzed on the basis of PLP score. The PLP scores for best docked conformation of 1,4-BQ, 1,4-NQ, 1,2-NQ, and 9,10-PQ were −27.06, −44.20, −44.67, and −59.05 against −102.57 of AMP-PNP. The $\Delta G_{binding}$ for 1,4-BQ, 1,4-NQ, 1,2-NQ, and 9,10-PQ were calculated as −577.67, −334.64, −162.69, and −671.89 kcal/mol against −435.96 kcal/mol of AMP-PNP. The key residues of binding site responsible for hydrogen bonding with AMP-PNP were identified to be Asn-91, Asn-120, Ser-148, Ser-149, Arg-162, Asn-163, Gly-164, Tyr-165, Gly-166, Ala-167, Lys-168, and Gln-376. The superposition of 1,4-BQ, 1,4-NQ, 1,2-NQ, and 9,10-PQ with AMP-PNP is

Downloaded from https://academic.oup.com/toxsci/article/126/2/372/1687885 by Ahmedabad University user on 01 May 2025

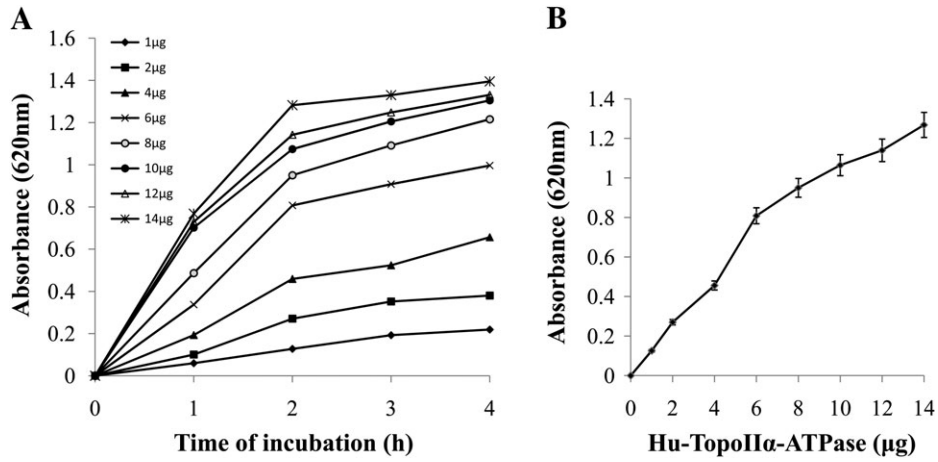



**FIG. 6.** (A) ATPase activity of Hu-TopoIIα determined by the malachite green assay as a function of time and protein. Each point is mean of three measurements. (B) Data from (A) plotted as Hu-TopoIIα-ATPase activity against protein for the 2-h time point with the error bars included.

shown in Figure 2A. The overall positioning of inhibitors is similar and overlaps near the ribose ring of the AMP-PNP (Figs. 2B–E). All the docked models of quinone-ATPase domain complexes are shown in Figures 3A–E. Hydrogen-bonding interactions were observed between oxygens attached to the aromatic ring of the quinones and –OH of Ser-148 and Ser-149 as well as $–NH_2$ of Asn-91 and Asn-150 (Figs. 4A–D). 1,4-BQ, 1,4-NQ, 1,2-NQ, and 9,10-PQ were also stabilized inside the active site through favorable van der Waals interactions with amino acid residues shown in Figure 5.

## ATPase Domain–Related Assay

### *Purification, Confirmation, and Kinetic Analysis of the Purified ATPase Domain of Hu-TopoIIα*

The entire scheme for purification is given in Supplementary figure 1. TEV protease was also purified for cleavage of His-MBP tag and is shown in Supplementary figure 4. The purified domain was confirmed by MALDI-TOF-TOF and LC-MS/MS analysis (Supplementary figures 2a and 2b). The protein was identified as AAG1303 of Homo sapiens with mascot score of 1269 having sequence coverage 34% (Supplementary figure 3). A 100% sequence match was observed with GENE ID: 7153TOP2A, topoisomerase (DNA) II alpha 170 kDa Homo sapiens using Basic Local Alignment Search Tool analysis.

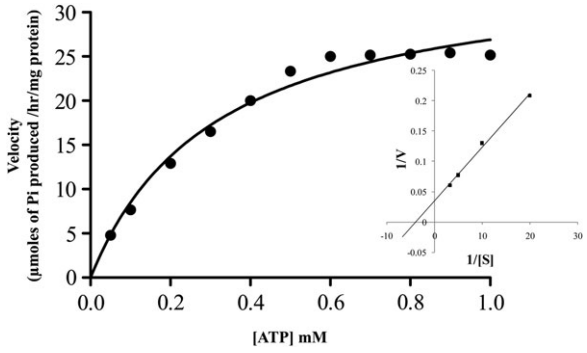



**FIG. 7.** Catalytic activity of the purified ATP-binding domain of Hu-TopoIIα following Michaelis-Menten equation. Double reciprocal Lineweaver-Burk plot (1/V) versus (1/S) is also shown.

The rate of ATP hydrolysis obtained for different time points (1–4 h) showed that this purified domain is kinetically active and displayed Michaelis-Menten kinetics (Fig. 6A). Linearity for release of inorganic phosphate from ATP hydrolysis by the purified Hu-TopoIIα-ATPase domain was observed up to 2 h at 37°C (Fig. 6B). A mean $K_m = 313.2 \pm 17.1\mu M$ (mean ± SE), $V_{max} = 35.41\mu M/min \pm 1.92\mu M$ (mean ± SE) of the purified ATPase domain was obtained (Fig. 7).

## Inhibition Assays for $IC_{50}$ Determination

To test our docking predictions, we investigated that whether 1,4-BQ, HQ, 1,2-NQ, 1,4-NQ, and 9,10-PQ inhibited ATPase domain in a dose-dependent manner. A concentration-dependent (0.1–50µM) inhibition of Hu-TopoIIα-ATPase activity was observed with BQ, 1,4-NQ, 1,2-NQ, and 9,10-PQ, respectively (Fig. 8A). However, hydroquinone showed inhibition at higher concentrations (< 400µM) as shown in Figure 8B. This is in agreement with recent findings that hydroquinone requires bioactivation for inhibition of the holoenzyme (Mondrala and Eastmond, 2010). The lowest $IC_{50}$ values were obtained for BQ (8.58 ± 0.8µM) as compared with 1,4-NQ (10.80 ± 0.72µM), 1,2-NQ (11.53 ± 2.08µM), 9,10-PQ (18.57 ± 0.66µM), and HQ (176.8 ± 4.56µM) (Table 1). All the compounds except HQ were found to be potent inhibitors of the ATPase domain. Subsequently, to decipher the mode of inhibition, we determined the apparent $K_m^{app}$ and $V_{max}^{app}$ in the presence of $IC_{50}$ concentrations of BQ. An increase in the $K_m$ was observed from 313.2 ± 17.1 to 828.6 ± 65.03µM ($K_m^{app}$, mean ± SE) with decrease in the $V_{max}$ from 35.41µM/min ± 1.92µM (mean ± SE) to 21.73 ± 1.53µM ($V_{max}^{app}$, mean ± SE) was observed. The inhibition data were further analyzed by nonlinear regression

Downloaded from https://academic.oup.com/toxsci/article/126/2/372/1687885 by Ahmedabad University user on 01 May 2025

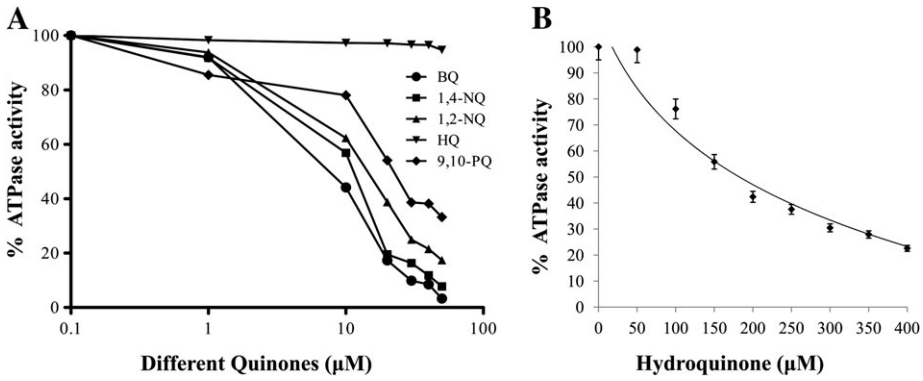



**FIG. 8.** Dose-response curve for inhibition of Hu-TopoIIα-ATPase domain activity by different quinones (A) inhibition by 1,4-benzoquinone, 1,4-naphthoquinone, 1,2-naphthoquinone, hydroquinone, and 9,10-phenanthroquinone. (B) Hydroquinone showing complete inhibition at 400μM. Data plotted are mean of three independent experiments.

analysis for identifying the best model (competitive, uncompetitive, or mixed inhibition). The analysis revealed that 1,4-BQ shows mixed inhibition for ATP hydrolysis and binds to the enzyme as well as enzyme substrate complex (Fig. 9). Thus, there appears to be at least two distinct binding sites for 1,4-BQ at the ATPase domain.

## Binding Studies by ITC

To add further evidence to the hypothesis and test whether these quinones effectively bind to the ATPase domain, ITC ligand-binding experiments were conducted. Binding characteristics of different compounds with Hu-TopoIIα-ATPase domain are shown in Figure 10. The binding constants of AMP-PNP and other compounds are given in Table 2. The isothermal binding curve fitted well to two sequentially site binding model for AMP-PNP with the $K_{a1}$ value ($10^4$) and $K_{a2}$ value ($10^3$), whereas the quinones were best fitted in four sequentially site binding model as evident from their statistical parameters (Table 2). The relative strength of binding (on the basis of average $K_d$ value calculated) was determined to be 1,4-BQ (4.24 ± 0.76μM) > 1,2-NQ (9.82 ± 0.93μM) > 1,4-NQ (9.41 ± 1.06μM) > 9,10-PQ (10.02 ± 0.90μM) > HQ (19.52 ± 4.97μM; Table 3). These findings are also consistent with our biochemical findings where 1,4-BQ exhibited strongest inhibition of the domain followed by 1,4-NQ > 1,2-NQ > 9,10-PQ > HQ. Based on these findings, the interaction site of 1,4-BQ at the catalytic step of the enzymes cycle is shown in Figure 11.

**TABLE 1**
**Potency of Inhibition in Screening Assay and $IC_{50}$ Values for Different Quinones**

| Compounds | % Inhibition at 40μM | $IC_{50}$ (μM) |
|---|---|---|
| 1,4-BQ | 96 | 8.58 ± 0.8 |
| 1,4-NQ | 89 | 10.80 ± 0.72 |
| 1,2-NQ | 80 | 11.53 ± 2.08 |
| 9,10-PQ | 64 | 18.57 ± 0.66 |
| HQ | 3 | 176.8 ± 4.56 |

*Note*. The values are average ± SD of three individual experiments. 1,4-BQ, Benzoquinone; 1,4-NQ, 1,4-naphthoquinone; 1,2-NQ, 1,2-naphthoquinone; 9,10-PQ, 9,10-phenanthroquinone; and HQ, hydroquinone.

## Cytotoxicity Assays

Both MTT and PI uptake assays revealed similar toxic responses for all the compounds as given below. Based on these observations, 1μM for 1h and 10μM for 30 min were taken as the highest possible concentration for further studies of all these quinones in BEAS-2B cells.

### *MTT Assay*

A statistically significant ($p < 0.05$) cytotoxic effect of different quinone compounds in human lung epithelial cells (BEAS-2B) was observed in MTT assay at concentrations (10–100μM) after 1-h exposure (Fig. 12A). All compounds except Et showed significant ($p < 0.05$; $p < 0.01$) reduction in

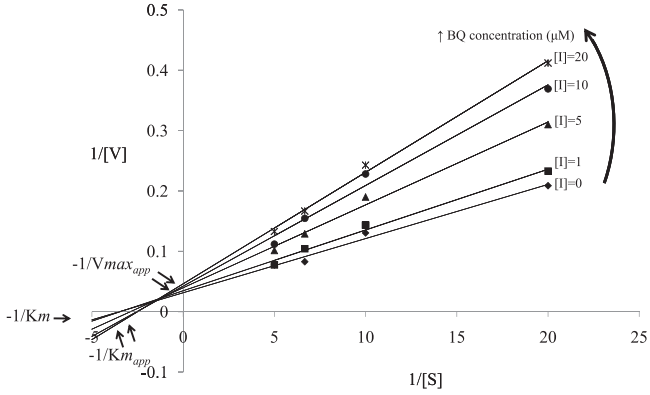



**FIG. 9.** Double reciprocal plot of 1/[V] versus 1/[S] in presence of increasing inhibitor 1,4-benzoquinone produced intersecting lines ($K_m^{app}$ and $V_{max}^{app}$) showing mixed inhibition.

Downloaded from https://academic.oup.com/toxsci/article/126/2/372/1687885 by Ahmedabad University user on 01 May 2025

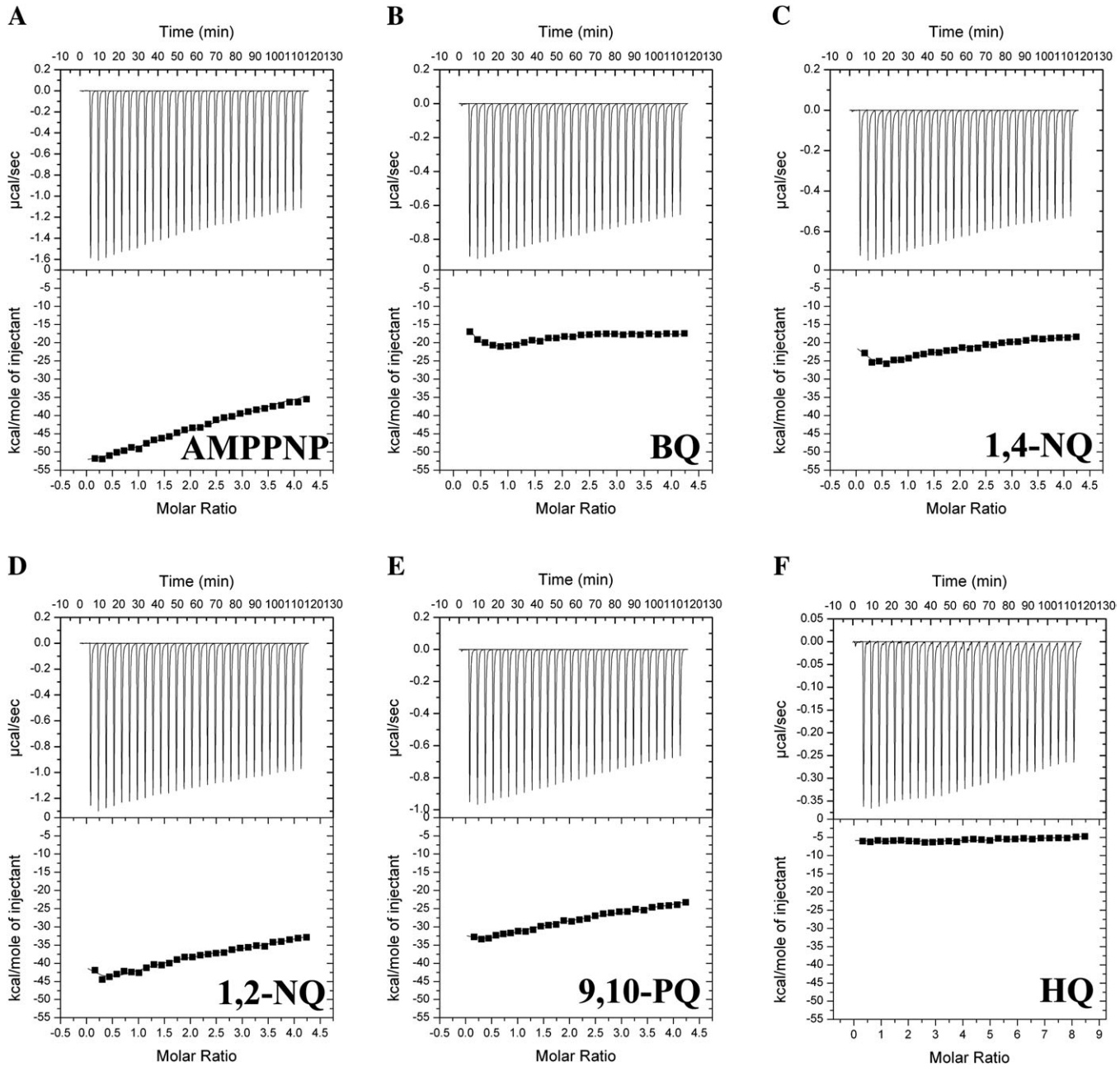



**FIG. 10.** Calorimetric titration for (A) adenosine 5′-(β,γ-imido) triphosphate, (B) 1,4-benzoquinone, (C) 1,4-naphthoquinone, (D) 1,2-naphthoquinone, (E) 9,10-phenanthroquinone, and (F) hydroquinone with purified Hu-TopoIIα-ATPase domain using ITC.

mitochondrial activity from 25μM. 1,4-NQ demonstrated maximum reduction of mitochondrial activity starting at 10μM concentration.

*Cytotoxicity Assay*

PI uptake assay revealed that 1,4-NQ showed ~42% cell death at 10μM concentration for 1 h. All other quinones showed statistically significant ($p < 0.05$; $p < 0.01$) cell death from 25μM concentration except 1,4-BQ (Fig. 12B).

## Cellular Localization of Hu-TopoIIα-DNA-Quinone Complexes

*Detection and Quantitation of Hu-TopoIIα-DNA-quinone Complexes*

Hu-TopoIIα-DNA-quinone complexes were observed in BEAS-2B after treatment with 1μM of 1,4-BQ, 1,4-NQ, 1,2-NQ, 9,10-PQ, and HQ (200μM) using TARDIS assay (Figs. 13A–G). A higher magnification (×100) for BEAS-2B cells shows the persistence of these complexes (cy3-red signals

Downloaded from https://academic.oup.com/toxsci/article/126/2/372/1687885 by Ahmedabad University user on 01 May 2025

**TABLE 2**
**Binding Constants ($K_a$) of AMP-PNP and Quinones With Hu-TopoIIα-ATPase Domain Obtained by ITC**

| Titration | $N$ | $K_a$, mol/l | $K_d = 1/K_a$ mol | $\Delta H$, cal/mol | $\Delta G = -RT\ln K_a$, cal/mol | $\Delta S = (\Delta H - \Delta G)/T$, cal/mol.K |
|---|---|---|---|---|---|---|
| AMP-PNP | 1 | $8.89 \pm 0.57 \times 10^4$ | $1.12 \pm 0.0721 \times 10^{-5}$ | $-1.693 \times 10^5 \pm 7.40 \times 10^3$ | −6861.34 | −536.1 |
| | 2 | $3.57 \pm 0.27 \times 10^3$ | $2.80 \pm 0.21 \times 10^{-4}$ | $-2.90 \times 10^6 \pm 2.11 \times 10^5$ | −4925.55 | −9554.7 |
| 1,4-1 | 1 | $5.24 \pm 0.49 \times 10^4$ | $1.91 \pm 0.18 \times 10^{-5}$ | $-1.154 \times 10^3 \pm 1.45 \times 10^3$ | −7929.48 | 22.34 |
| | 2 | $5.64 \pm 0.54 \times 10^5$ | $1.77 \pm 0.17 \times 10^{-6}$ | $-1.488 \times 10^5 \pm 1.07 \times 10^4$ | −7973.78 | −464.94 |
| | 3 | $1.40 \pm 0.14 \times 10^5$ | $7.14 \pm 0.71 \times 10^{-6}$ | $2.295 \times 10^5 \pm 1.90 \times 10^4$ | −7134.78 | 783.74 |
| | 4 | $7.42 \pm 0.86 \times 10^4$ | $1.35 \pm 0.16 \times 10^{-5}$ | $-4.026 \times 10^5 \pm 1.51 \times 10^4$ | −6752.5 | −1305.17 |
| 1,4-NQ | 1 | $7.7 \pm 0.81 \times 10^4$ | $1.3 \pm 0.14 \times 10^{-5}$ | $-7.682 \times 10^4 \pm 5.79 \times 10^3$ | −6774.81 | −231.17 |
| | 2 | $1.41 \pm 0.15 \times 10^5$ | $7.09 \pm 0.75 \times 10^{-6}$ | $-8.570 \times 10^4 \pm 1.34 \times 10^4$ | −7139.06 | −259.28 |
| | 3 | $9.49 \pm 1.3 \times 10^4$ | $1.05 \pm 0.14 \times 10^{-5}$ | $2.199 \times 10^5 \pm 3.20 \times 10^4$ | −6900.66 | 748.52 |
| | 4 | $1.23 \pm 0.13 \times 10^5$ | $8.13 \pm 0.86 \times 10^{-6}$ | $-3.198 \times 10^5 \pm 2.89 \times 10^4$ | −7056.83 | −1078.74 |
| 1,2-NQ | 1 | $1.07 \pm 0.1 \times 10^5$ | $9.35 \pm 0.87 \times 10^{-6}$ | $-1.183 \times 10^5 \pm 7.13 \times 10^4$ | −6972.92 | −367.42 |
| | 2 | $1.04 \pm 0.096 \times 10^5$ | $9.61 \pm 0.89 \times 10^{-6}$ | $-1.232 \times 10^5 \pm 1.63 \times 10^4$ | −6955.8 | −383.64 |
| | 3 | $9.17 \pm 1.1 \times 10^4$ | $1.09 \pm 0.13 \times 10^{-5}$ | $2.192 \times 10^5 \pm 4.15 \times 10^4$ | −6880.01 | 746.14 |
| | 4 | $1.05 \pm 0.085 \times 10^5$ | $9.52 \pm 0.77 \times 10^{-6}$ | $-4.254 \times 10^5 \pm 3.38 \times 10^4$ | −6961.56 | −1380.98 |
| 9,10-PQ | 1 | $1.04 \pm 0.094 \times 10^5$ | $9.61 \pm 0.87 \times 10^{-6}$ | $-9.470 \times 10^4 \pm 5.47 \times 10^3$ | −6955.8 | −289.58 |
| | 2 | $8.35 \pm 0.72 \times 10^4$ | $1.2 \pm 0.10 \times 10^{-5}$ | $-9.726 \times 10^4 \pm 1.38 \times 10^4$ | −6823.6 | −343.51 |
| | 3 | $1.29 \pm 0.1 \times 10^5$ | $7.75 \pm 0.60 \times 10^{-6}$ | $1.474 \times 10^5 \pm 2.39 \times 10^4$ | −7085.51 | 509.85 |
| | 4 | $8.84 \pm 1.0 \times 10^4$ | $1.13 \pm 0.13 \times 10^{-5}$ | $-2.718 \times 10^5 \pm 2.23 \times 10^4$ | −6857.94 | −874.4 |
| HQ | 1 | $2.38 \pm 0.76 \times 10^5$ | $4.20 \pm 1.34 \times 10^{-6}$ | $-1.080 \times 10^4 \pm 1.54 \times 10^3$ | −7454.28 | −11.04 |
| | 2 | $5.76 \pm 1.5 \times 10^4$ | $1.74 \pm 0.45 \times 10^{-5}$ | $-2.612 \times 10^4 \pm 6.90 \times 10^3$ | −6600.02 | −64.42 |
| | 3 | $1.50 \pm 0.37 \times 10^4$ | $6.67 \pm 1.64 \times 10^{-5}$ | $-4.603 \times 10^4 \pm 3.33 \times 10^4$ | −5789.88 | −132.81 |
| | 4 | $3.35 \pm 0.7 \times 10^4$ | $2.98 \pm 0.62 \times 10^{-5}$ | $-4.478 \times 10^4 \pm 3.70 \times 10^4$ | −6273.68 | −127.08 |

*Note*. The values are average of three individual experiments. $N$, number of sequential binding sites; $K_a$, Association constant; $\Delta H$, change in enthalpy; $\Delta S$, change in entropy; $\Delta G$, Gibbs free energy change; AMP-PNP (non-hydrolyzable ATP analog); 1,4-BQ, benzoquinone; 1,4-NQ, 1,4-naphthoquinone; 1,2-NQ, 1,2-naphthoquinone; 9,10-PQ, 9,10-phenanthroquinone; and HQ, hydroquinone.

for Ki-S1 monoclonal antibody specific for Hu-TopoIIα only) inside the nuclei (DAPI-blue stained; Figs. 14A–F). The fluorescence measurements of cy3-labeled secondary antibody specific for antihuman topoisomerase IIα (Ki-S1) in BEAS-2B cells for compounds (Et, 1,4-BQ, 1,4-NQ, 1,2-NQ, and 9,10-PQ) were done at 1μM. An increase in the fluorescence corresponding to quinone-stabilized Hu-TopoIIα-DNA complexes was in the order Et > BQ > 1,4-NQ > 1,2-NQ > PQ (Fig. 15) and was consistent with our biochemical findings.

**TABLE 3**
**Average Binding Constants Obtained for All Quinones Using ITC**

| Compounds | Average $K_d$ value (μM) |
|---|---|
| 1,4-BQ | 4.24 ± 0.76 |
| 1,4-NQ | 9.41 ± 1.06 |
| 1,2-NQ | 9.82 ± 0.93 |
| 9,10-PQ | 10.02 ± 0.90 |
| HQ | 19.52 ± 4.97 |

*Note*. The values are average ± SD of three independent experiments. 1,4-BQ, 1,4-benzoquinone; 1,4-NQ, 1,4-naphthoquinone; 1,2-NQ, 1,2-naphthoquinone; 9,10-PQ, 9,10-phenanthroquinone; and HQ, hydroquinone.

### *γ-H2A.X Detection in BEAS-2B Cells*

*Quantitation of γ-H2A.X by flow cytometry*. A quantitative concentration–dependent increase in the γ-H2A.X levels was observed in BEAS-2B cells treated with different quinone compounds (1,4-BQ, 1,4-NQ, 1,2-NQ, 9,10-PQ, HQ) with

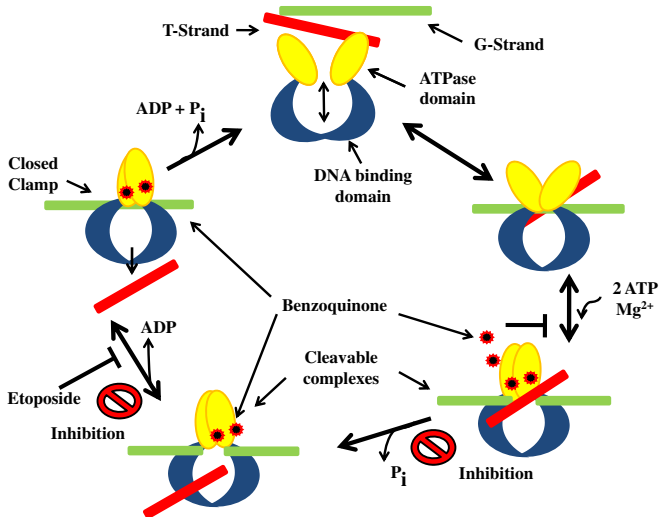



**FIG. 11.** Inhibitory action of 1,4-benzoquinone restricting ATPase domain movement during catalytic cycle of topoisomerase IIα.

Downloaded from https://academic.oup.com/toxsci/article/126/2/372/1687885 by Ahmedabad University user on 01 May 2025

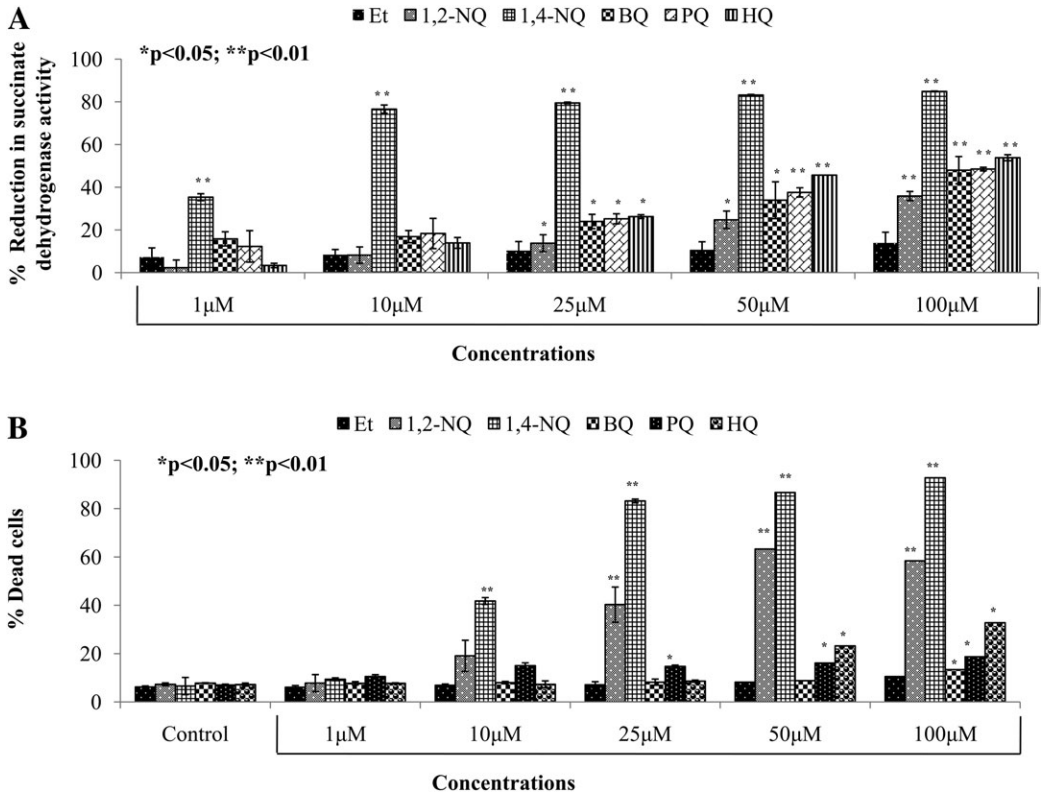



**FIG. 12.** Cytotoxicity induced by different concentrations of quinone compounds in BEAS-2B cells (A) MTT assay (B) PI staining. Data plotted are mean ± SD of three independent experiments.

a highly significant ($p < 0.001$) response at 10μM concentration corresponding to DNA DSBs accumulated inside cells. However, the increase was not as marked in PQ and was nonsignificant in HQ-treated cells at this concentration (Fig. 16).

*Immunocytochemical visualization of γ-H2A.X.* A qualitative concentration–dependent increase in the signal of γ-H2A.X was also observed in the BEAS-2B cells treated with Et and comparatively strongest inhibitor 1,4-BQ (Figs. 17A–H). The green signals for primary FITC-labeled anti-γ-H2A.X antibody were evident in a dose-dependent manner. Therefore, these quinones display the potential of generating Hu-TopoIIα-mediated DSBs inside the cells.

## DISCUSSION

The present study shows that the environmentally relevant quinones, such as 1,4-benzoquinone, naphthoquinones, and phenanthroquinone, act as catalytic inhibitors of the ATPase domain of Hu-TopoIIα. Previously, it has been reported that the toxicity of quinones is due to their electrophilic nature, thereby forming covalent adducts with proteins via 1,4-addition chemistry. Although quinones act as either electrophiles or redox-cycling agents, the degree to which these properties contribute to their toxicity mechanisms is unclear and is also significantly dependent on individual chemical properties and the experimental conditions. Therefore, other yet uncharacterized mechanisms of quinone toxicity may be marked by the presumption that all quinone-mediated interactions are solely the result of these two mechanisms. Quinones act as topo II poison by inhibiting the decatenation and relegation activity of Hu-TopoIIα. Baker *et al.* (2001), in an *in vitro* study, have shown that quinones act as potent inhibitors of Hu-TopoIIα relative to that of etoposide. These compounds induce the formation and accumulation of DSBs leading to apoptosis (Lu *et al.* 2005). One of the many mechanisms of action of quinones on Hu-TopoIIα could be due to a distinct mode of action on its ATPase domain that hydrolyzes ATP and helps in domain movements essential for catalytic activity of the enzyme (Cai *et al.*, 2008; Li *et al.*, 2010). Catalytic cycle of the enzyme includes strand passage of duplex DNA, thereby relieving the torsional stress during vital cellular processes, such as transcription, replication, repair, chromatin remodeling, etc. Elucidation of quinone-Hu-TopoIIα ATPase domain interactions would therefore offer a clear understanding of the genotoxic effects mediated by the enzyme's inhibition.

Until now, a detailed interaction mechanism between the quinone inhibitors and ATPase domain has not been completely elucidated, due to unavailability of the crystal structure of these complexes. Utilizing the rapid advances in

Downloaded from https://academic.oup.com/toxsci/article/126/2/372/1687885 by Ahmedabad University user on 01 May 2025

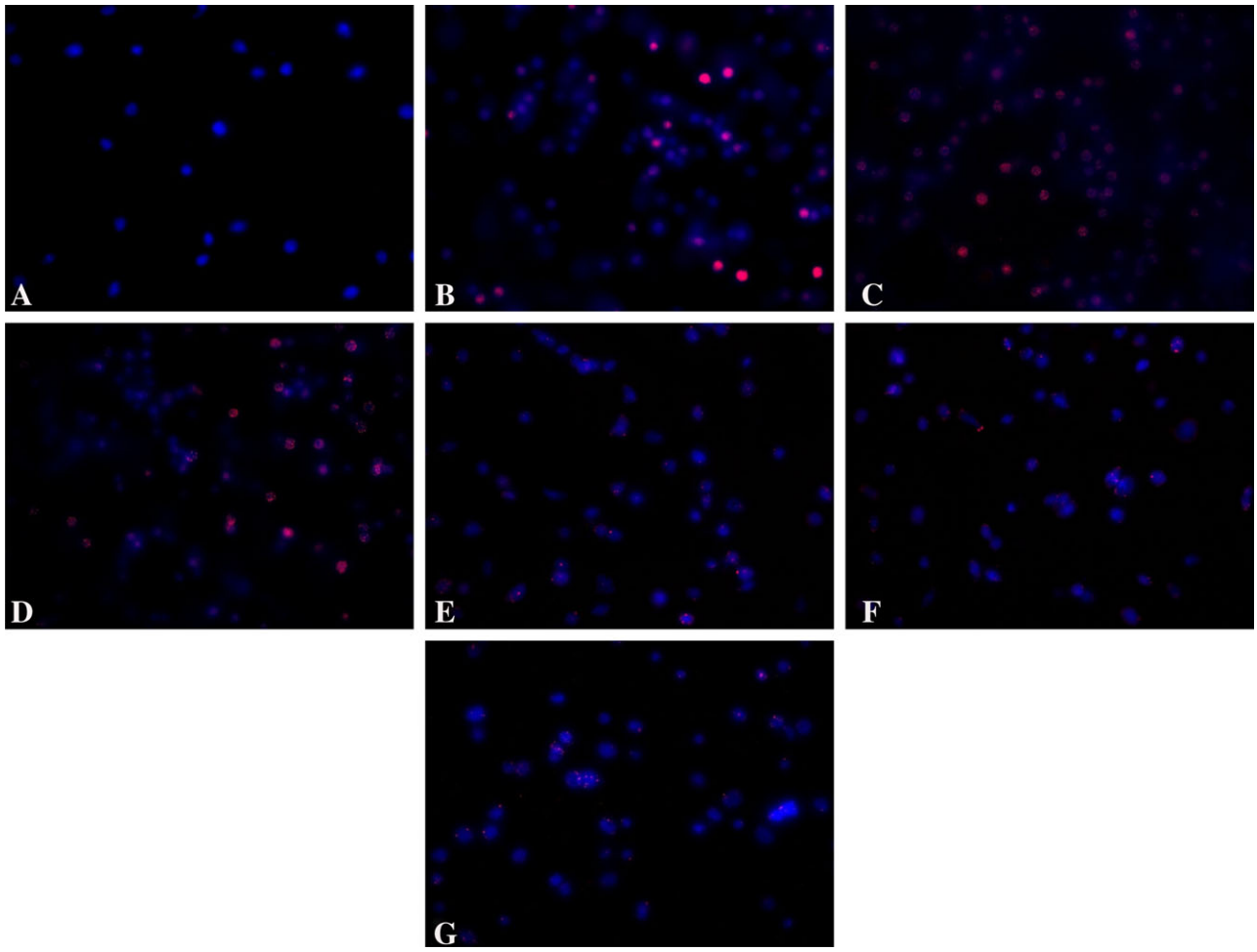



**FIG. 13.** Representative immunofluorescence images of treated BEAS-2B cells for detection of quinone-stabilized Hu-TopoIIα-DNA complexes using TARDIS assay. Cells were treated with 1μM of different compounds for 1 h. Hu-TopoIIα-DNA complexes were detected using anti-topoisomerase IIα (Ki-S1) and Cy3-conjugated second antibody. DAPI-stained DNA (blue) and Cy3-stained (red) immunofluorescence for Hu-TopoIIα were observed due to quinone-stabilized cleavable complexes. Etoposide was used as positive control. (All images were captured using ×10 objective and were typical of those seen in replicate experiments). (A) Control, (B) Etoposide (1μM), (C) 1,4-benzoquinone (1μM), (D) 1,4-naphthoquinone (1μM), (E) 1,2-naphthoquinone (1μM), (F) 9,10-phenanthroquinone (1μM), and (G) hydroquinone (1μM).

molecular docking and characterized crystal structures with the cocrystallized ligand, accurate prediction of the binding mode between these quinones and ATP-binding site can be made (Paul and Rognan, 2002). Such molecular docking studies have been previously performed with salvicine (a diterpenoid quinone) and emodin (similar to 1,4-anthraquinone), targeting the ATPase domain of Hu-TopoIIα. It has been shown that these quinones are capable of interacting via hydrogen-bonding interactions with several active site residues (Cai *et al*., 2008).

To understand the precise interactions of quinones with the amino acid residues of the ATP-binding pocket, computational modeling studies were carried out to understand the molecular basis of ATPase domain inhibition. Crystal structure of ATPase domain of Hu-TopoIIα, complexed with AMP-PNP (pdb code: 1ZXM), was used. Our molecular docking studies revealed that these quinone compounds (1,4-BQ, 1,4-NQ, 1,2-NQ, and 9,10-PQ) dock at position very close to ribose ring of the original cocrystallized ligand AMP-PNP. Also, the oxygens attached at 1,2- (ortho) or 1,4- (para) position to the aromatic ring of these quinone compounds participate in hydrogen bonding and van der Waals interactions with key active site residues. The binding energies of these quinone compounds with the ATPase domain were found in the order 9,10 PQ > 1,4-BQ > 1,4-NQ > 1,2-NQ. Thus, our *in silico* findings provided data suggesting that 1,4-BQ, 1,4-NQ, 1,2-NQ, and 9,10-PQ might inhibit the ATPase domain in a distinct manner. The interaction modes demonstrated the dynamic aspects of quinone-ATPase domain complex and helps in understanding the inhibitory action of these compounds. Therefore, the inhibition of this domain would profoundly affect the enzymes catalytic cycle leading to bridging of the ATPase

Downloaded from https://academic.oup.com/toxsci/article/126/2/372/1687885 by Ahmedabad University user on 01 May 2025

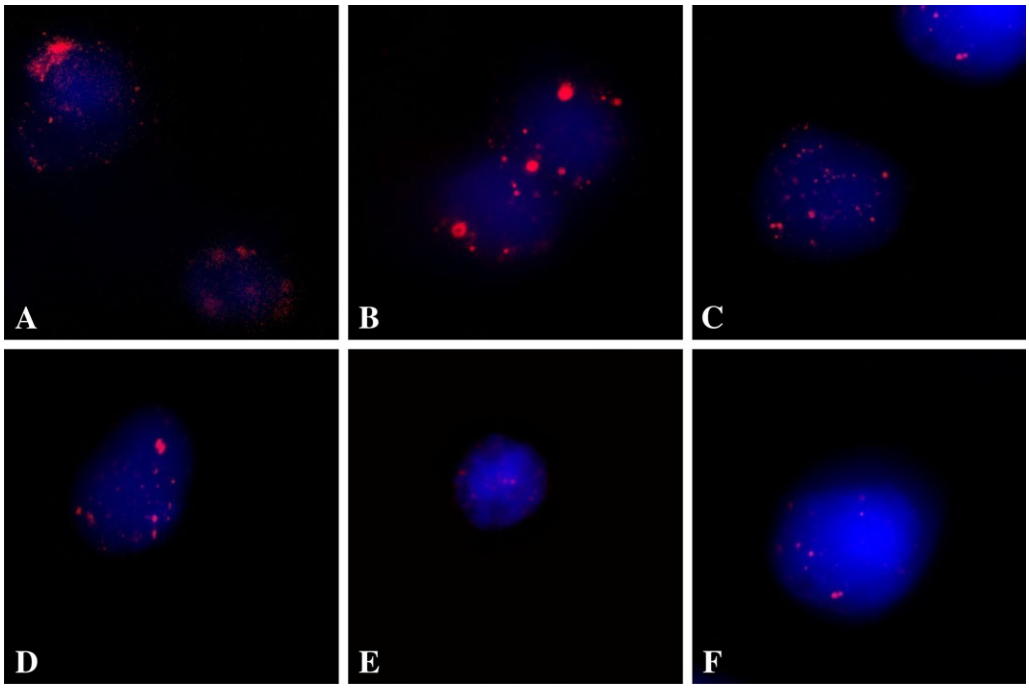



**FIG. 14.** Representative immunofluorescence images of treated BEAS-2B cells at higher magnification showing signals for quinone-stabilized Hu-TopoIIα-DNA complexes. (A) Etoposide (1μM), (B) 1,4-benzoquinone (1μM), (C) 1,4-naphthoquinone (1μM), (D) 1,2-naphthoquinone (1μM), (E) 9,10-phenanthroquinone (1μM), and (F) hydroquinone (1μM). All images were captured at ×100 magnification using oil immersion objective ×63 and were typical of those seen in replicate experiments.

domains and stabilizing the enzyme at the cleavage complex stage and at closed clamp configuration.

Therefore, in further support to this theory, ATPase domain was purified and found to be kinetically active. Analysis of the ATP hydrolysis rates for ATPase domain of Hu-TopoIIα showed that it obeys Michaelis-Menten kinetics with $K_m$ value (0.313mM) comparable to that previously reported (0.350mM)

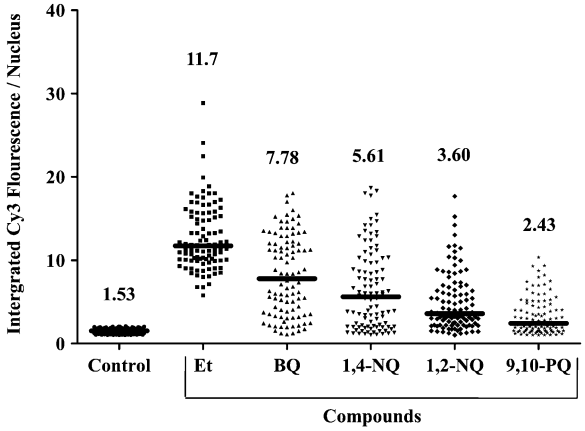



**FIG. 15.** Scattergram showing comparative fluorescence levels of Hu-TopoIIα signal derived from quinone-treated BEAS-2B cells. Etoposide (Et), 1,4-benzoquinone, 1,4-naphthoquinone, 1,2-naphthoquinone, and 9,10-phenenthrenequinone. Each specific marker dot represents the integrated fluorescence value of a single nucleus for single compound. The horizontal lines represent the median values.

by Hu *et al.* (2002). Biochemical inhibition studies using malachite green assay showed that 1,4-BQ is the most potent inhibitor followed > 1,4-NQ > 1,2-NQ > 9,10-PQ > HQ, as evident from their $IC_{50}$ values. Interestingly, 9,10-PQ did not completely inhibit the ATP hydrolysis activity when compared with the other quinones, which indicates that it might interact allosterically with the enzyme. The interactions energies calculated from computationally derived models are well correlated with $IC_{50}$ values obtained for ATPase activity inhibition except 9,10-PQ. One possible reason could be that 9,10-PQ has low electrophilicity when compared with 1,4-BQ, 1,4-NQ, and 1,2-NQ as previously reported (Rodriguez *et al.*, 2004) and also showed differential toxicity effects in their study. Other reason could be due to the differences in the entropic contributions during the binding of these quinones inside the active site, which cannot be neglected and are shown in Table 2. The higher $IC_{50}$ for HQ could be attributed to the fact that it requires bioactivation by myeloperoxidase as observed by Eastmond *et al.* (2005). To establish the mechanism of inhibition of the ATPase domain, double reciprocal plots were used for analyzing the effect of 1,4-BQ (strongest inhibitor) at different ATP concentrations. The data showed that the 1,4-BQ is a mixed inhibitor of the Hu-TopoIIα-ATPase domain (evident from the increase in apparent $K_m^{app}$ and decrease in $V_{max}^{app}$ in the presence of $IC_{50}$ concentration of 1,4-BQ). Such inhibition results from binding of the molecule to the enzyme at distant sites as well

Downloaded from https://academic.oup.com/toxsci/article/126/2/372/1687885 by Ahmedabad University user on 01 May 2025

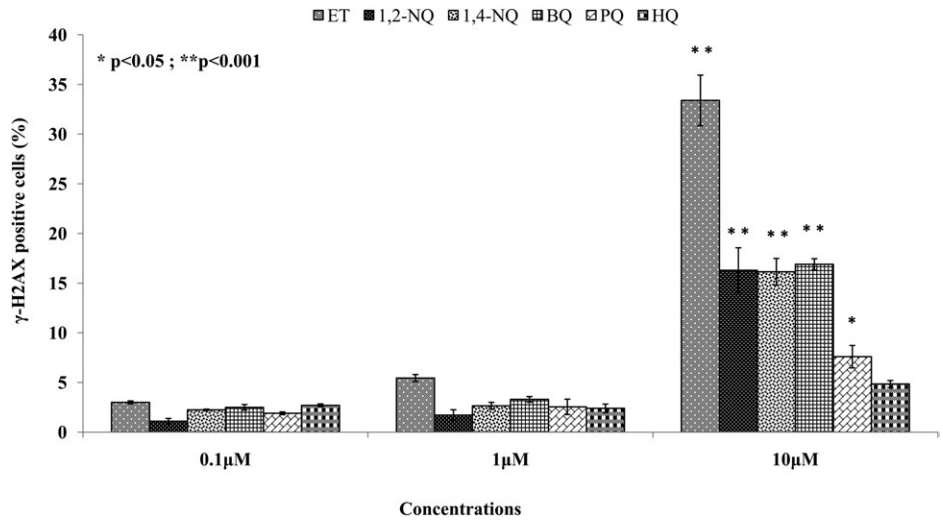



**FIG. 16.** Dose-dependent response for relative γ-H2A.X signals in BEAS-2B cells induced by different quinones (1,4-benzoquinone, 1,4-naphthoquinone, 1,2-naphthoquinone, 9,10-phenenthroquinone, hydroquinone, and etoposide). Data plotted are mean ± SD of three independent experiments.

as enzyme-substrate complex site. The action of BQ at this catalytic step of the enzyme cycle is shown in Figure 7.

The ITC is a sensitive method for measuring and comparing the thermodynamic parameters associated with binding of different ligands to their receptors. In the present study, data from the ITC experiments showed that 1,4-BQ exhibits significantly higher affinity for the ATPase domain of Hu-TopoIIα in comparison with other ligands. The order of binding was found to be 1,4-BQ > 1,4-NQ > 1,2-NQ > 9,10-PQ. This order is consistent with the $K_m$ values obtained biochemically for these ligands. The binding of quinones to the ATPase domain corresponds to the favorable Gibbs free energy changes as shown in Table 2. Out of four sequentially site binding, three sites offer negative $\Delta H$ and $\Delta S$ values and fourth one has a positive $\Delta H$ and $\Delta S$ value. The contribution of enthalpy and entropy is additive for three of four binding sites. This is because of the structures of the ligands, which allow for both enthalpic interactions like hydrogen bonding, and van der Waals interaction involving the ring systems, which is an entropy-driven process. For one of the binding sites, there is enthalpy-entropy compensation. Molecular modeling results were also consistent with ITC data, as these quinones are stabilized inside the active site by forming hydrogen bonds with amino acid residues. However, the $\Delta H$ and $\Delta S$ values cannot be directly correlated with the docked models. Nevertheless, comparisons were made from the averaged $K_d$ values, and the results were consistent with *in silico* and biochemical findings. From the results from the *in silico*, biochemical, and ITC studies, it can be inferred that at least in part, these quinone compounds share a common binding site with AMP-PNP.

It therefore appears that the inhibitory and clastogenic effects of the quinones could be at least in part as a result of halt of the enzyme function at the stages where ATP hydrolysis occurs, i.e., first at cleavage complex formation and second at

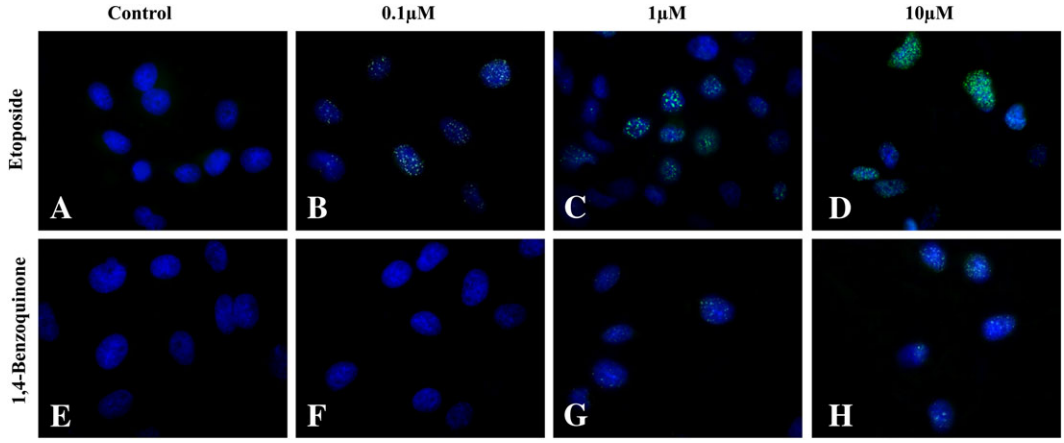



**FIG. 17.** Immunocytochemical detection of FITC-labeled γ-H2A.X primary antibody signals in BEAS-2B cells induced by etoposide (A–D) and 1,4-benzoquinone (E–H).

Downloaded from https://academic.oup.com/toxsci/article/126/2/372/1687885 by Ahmedabad University user on 01 May 2025

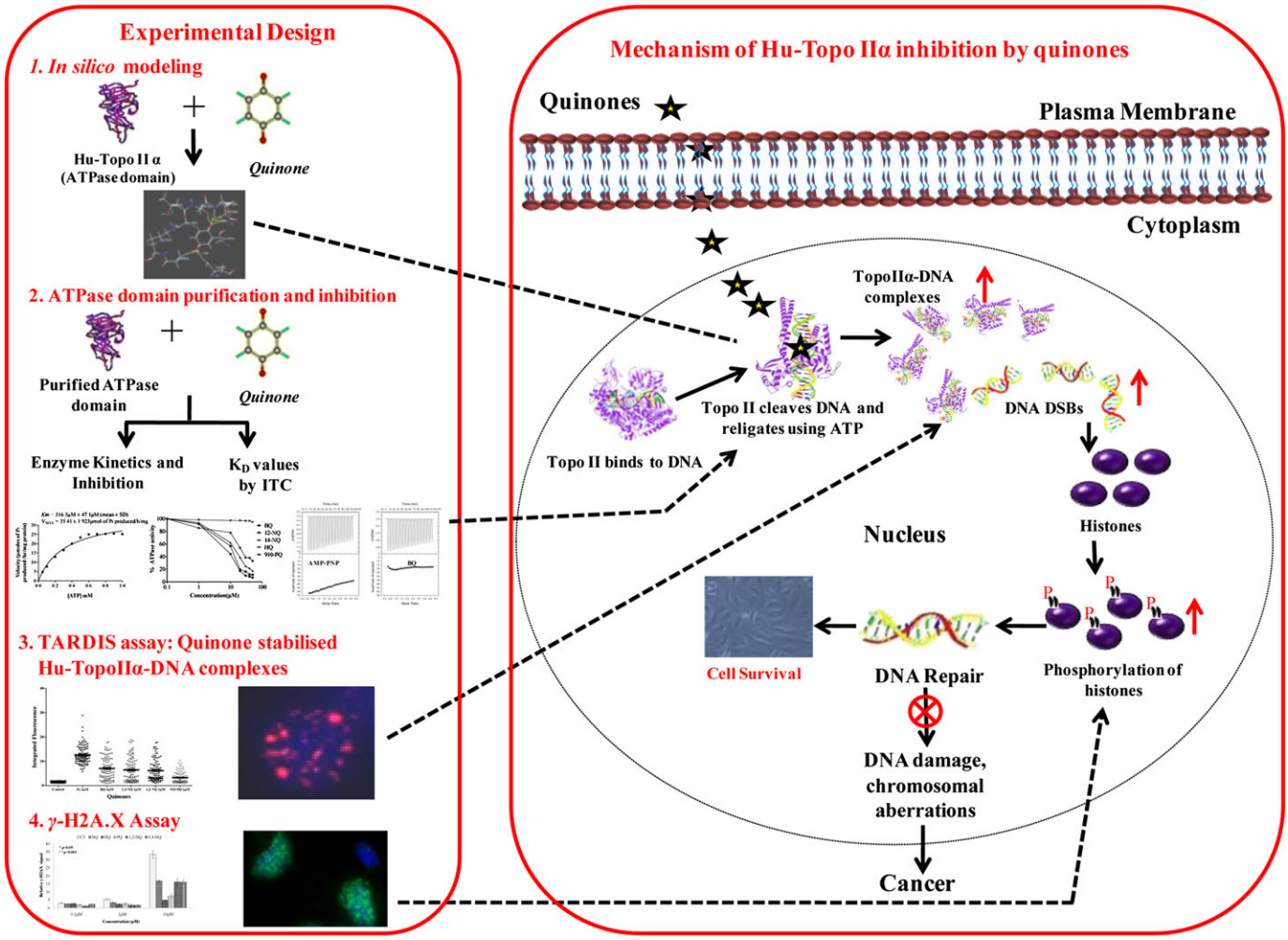



**FIG. 18.** Schematic representation showing inhibition of ATPase domain of Hu-TopoIIα by 1,4-benzoquinone, 1,4-naphthoquinone, 1,2-naphthoquinone, and 9,10-phenanthroquinone leads to accumulation of stabilized TopoIIα complexes and DNA DSBs inside cells.

closed complex configuration. Hydrolysis of one ATP with concomitant release of the hydrolyzed phosphate induces the passage of the T-strand of DNA through the G-strand promoting the relegation of the G-strand and release of the T-strand through the C-terminal gate of the enzyme and formation of a closed clamp configuration. The hydrolysis of the second ATP then occurs for dissociation of the dimerized ATPase domains for the enzymes next catalytic cycle (Mondrala and Eastmond, 2010). Such an inhibitory action would therefore lead to the accumulation of quinone-stabilized Hu-TopoIIα-DNA complexes leading to DNA DSBs inside the cells.

To test this theory, BEAS-2B cell line was chosen for persistence of quinone-stabilized Hu-TopoIIα-DNA complexes. This cell line has been previously used for testing the carcinogenic potential of chemicals (Nichols *et al.*, 1995). Immortalized human bronchial epithelial cell culture BEAS-2B also serves as a good *in vitro* model for inhalation exposure to environmental carcinogens with a high metabolic capacity (van Agen *et al.*, 1997). Lung is also the major organ exposed to these environmentally occurring quinones. In the present study, the noncytotoxic concentrations of the compounds were used for *in vitro* experiments. TARDIS assay revealed that 1,4-BQ maximally induced quinone-stabilized Hu-TopoIIα-DNA complexes followed by 1,4-NQ > 1,2-NQ > 9,10-PQ > HQ. The data reaffirm that quinones are capable of producing cleavable complexes produced mainly due to inhibition of relegation activity of Hu-TopoIIα, thereby adding weight of evidence to our hypothesis. It has been shown that these complexes further lead to the accumulation of DNA DSBs (Lynch *et al.*, 2003) due to restriction of domain movement.

The formation of DNA-DSBs (DNA-DSBs) triggers the phosphorylation of histone at Ser-139 (H2A.X, a marker of DNA-DSBs), thereby leading to the recruitment of DNA repair factors at the site of damage (Paull *et al.*, 2000). It has been further studied that a positive correlation occurs between the formation of DNA-DSBs and γ-H2A.X levels in response to etoposide (Smart *et al.*, 2008). To further investigate the role

Downloaded from https://academic.oup.com/toxsci/article/126/2/372/1687885 by Ahmedabad University user on 01 May 2025

of quinone-stabilized Hu-TopoIIα associated DNA-DSBs, formation of γ-H2A.X was assessed in BEAS-2B cells. Our results showed a concentration-dependent increase in γ-H2A.X levels for etoposide and 1,4-BQ as evident by FITC-labeled primary anti-phospho-histone antibody (green signals inside cells in Fig. 17). Comparative quantitative responses were also observed for γ-H2A.X levels by flow cytometry. A significant increase in the γ-H2A.X formation inside BEAS-2B cells corresponds to the accumulation of DNA DSBs, which at least in part are associated with inhibition of Hu-TopoIIα. 1,4-BQ produced maximum response while HQ exhibited the least signals when compared with etoposide as positive control. This was also in agreement with our other experimental findings. A schematic presentation of the mechanism of inhibition of ATPase domain of the enzyme and dominant cellular consequences observed is presented in Figure 18.

In conclusion, the study provides evidence on the role of Hu-TopoIIα in the clastogenic responses induced by environmentally occurring quinones.

## SUPPLEMENTARY DATA

Supplementary data are available online at http://toxsci.oxfordjournals.org/.

## FUNDING

Council of Scientific and Industrial Research (CSIR), New Delhi under its Network Project (NWP34) and Supra Institutional Project (SIP-08).

## ACKNOWLEDGMENTS

D.G. thanks the CSIR, New Delhi for the award of Senior Research Fellowship. The authors declare that there are no conflicts of interest.

## REFERENCES

Baker, R. K., Kurz, E. U., Pyatt, D. W., Irons, R. D., and Kroll, D. J. (2001). Benzene metabolites antagonize etoposide-stabilized cleavable complexes of DNA topoisomerase II alpha. *Blood* **98,** 830–833.

Bender, R. P., Ham, A. J., and Osheroff, N. (2007). Quinone-induced enhancement of DNA cleavage by human topoisomerase IIalpha: Adduction of cysteine residues 392 and 405. *Biochemistry* **46,** 2856–2864.

Boege, F., Andersen, A., Jensen, S., Zeidler, R., and Kreipe, H. (1995). Proliferation-associated nuclear antigen Ki-S1 is identical with topoisomerase II alpha. Delineation of a carboxy-terminal epitope with peptide antibodies. *Am. J. Pathol.* **146,** 1302–1308.

Bolton, J. L., Trush, M. A., Penning, T. M., Dryhurst, G., and Monks, T. J. (2000). Role of quinones in toxicology. *Chem. Res. Toxicol.* **13,** 135–160.

Bradford, M. M. (1976). A rapid and sensitive method for the quantitation of microgram quantities of protein utilizing the principle of protein-dye binding. *Anal. Biochem.* **72,** 248–254.

Cai, Y. J., Lu, J. J., Zhu, H., Xie, H., Huang, M., Lin, L. P., Zhang, X. W., and Ding, J. (2008). Salvicine triggers DNA double-strand breaks and apoptosis by GSH-depletion-driven $H_2O_2$ generation and topoisomerase II inhibition. *Free Radic. Biol. Med.* **45,** 627–635.

Eastmond, D. A., Mondrala, S. T., and Hasegawa, L. (2005). Topoisomerase II inhibition by myeloperoxidase-activated hydroquinone: A potential mechanism underlying the genotoxic and carcinogenic effects of benzene. *Chem. Biol. Interact.* **153–154,** 207–216.

Hu, C. X., Zuo, Z. L., Xiong, B., Ma, J. G., Geng, M. Y., Lin, L. P., Jiang, H. L., and Ding, J. (2006). Salvicine functions as novel topoisomerase II poison by binding to ATP pocket. *Mol. Pharmacol.* **70,** 1593–1601.

Hu, T., Sage, H., and Hsieh, T. S. (2002). ATPase domain of eukaryotic DNA topoisomerase II. Inhibition of ATPase activity by the anti-cancer drug bisdioxopiperazine and ATP/ADP-induced dimerization. *J. Biol. Chem.* **277,** 5944–5951.

Kepley, C. L., Lauer, F. T., Oliver, J. M., and Burchiel, S. W. (2003). Environmental polycyclic aromatic hydrocarbons, benzo(a) pyrene (BaP) and BaP-quinones, enhance IgE-mediated histamine release and IL-4 production in human basophils. *Clin. Immunol.* **107,** 10–19.

Li, Y., Luan, Y., Qi, X., Li, M., Gong, L., Xue, X., Wu, X., Wu, Y., Chen, M., Xing, G., *et al.* (2010). Emodin triggers DNA double-strand breaks by stabilizing topoisomerase II-DNA cleavage complexes and by inhibiting ATP hydrolysis of topoisomerase II. *Toxicol. Sci.* **118,** 435–443.

Lindsey, R. H., Jr, Bromberg, K. D., Felix, C. A., and Osheroff, N. (2004). 1,4-Benzoquinone is a topoisomerase II poison. *Biochemistry* **43,** 7563–7574.

Lu, H. R., Zhu, H., Huang, M., Chen, Y., Cai, Y. J., Miao, Z. H., Zhang, J. S., and Ding, J. (2005). Reactive oxygen species elicit apoptosis by concurrently disrupting topoisomerase II and DNA-dependent protein kinase. *Mol. Pharmacol.* **68,** 983–994.

Lynch, A., Harvey, J., Aylott, M., Nicholas, E., Burman, M., Siddiqui, A., Walker, S., and Rees, R. (2003). Investigations into the concept of a threshold for topoisomerase inhibitor-induced clastogenicity. *Mutagenesis* **18,** 345–353.

Mondrala, S., and Eastmond, D. A. (2010). Topoisomerase II inhibition by the bioactivated benzene metabolite hydroquinone involves multiple mechanisms. *Chem. Biol. Interact.* **184,** 259–268.

Mosmann, T. (1983). Rapid colorimetric assay for cellular growth and survival: Application to proliferation and cytotoxicity assays. *J. Immunol. Methods* **65,** 55–63.

Mueller-Planitz, F., and Herschlag, D. (2008). Coupling between ATP binding and DNA cleavage by DNA topoisomerase II: A unifying kinetic and structural mechanism. *J. Biol. Chem.* **283,** 17463–17476.

Muslimovic, A., Ismail, I. H., Gao, Y., and Hammarsten, O. (2008). An optimized method for measurement of gamma-H2AX in blood mononuclear and cultured cells. *Nat. Protoc.* **3,** 1187–1193.

Nichols, W. K., Terry, C. M., Cutler, N. S., Appleton, M. L., Jesthi, P. K., and Yost, G. S. (1995). Oxidation at C-1 controls the cytotoxicity of 1,1-dichloro-2,2- bis(p-chlorophenyl)ethane by rabbit and human lung cells. *Drug Metab. Dispos.* **23,** 595–599.

O'Brien, M. C., and Bolton, W. E. (1995). Comparison of cell viability probes compatible with fixation and permeabilization for combined surface and intracellular staining in flow cytometry. *Cytometry* **19,** 243–255.

Pandey, A. K., Gurbani, D., Bajpayee, M., Parmar, D., Ajmani, S., and Dhawan, A. (2009). In silico studies with human DNA topoisomerase-II alpha to unravel the mechanism of in vitro genotoxicity of benzene and its metabolites. *Mutat. Res.* **661,** 57–70.

Paul, N., and Rognan, D. (2002). ConsDock: A new program for the consensus analysis of protein-ligand interactions. *Proteins* **47,** 521–533.

Paull, T. T., Rogakou, E. P., Yamazaki, V., Kirchgessner, C. U., Gellert, M., and Bonner, W. M. (2000). A critical role for histone H2AX in recruitment of repair factors to nuclear foci after DNA damage. *Curr. Biol.* **10,** 886–895.

Downloaded from https://academic.oup.com/toxsci/article/126/2/372/1687885 by Ahmedabad University user on 01 May 2025

Rodriguez, C. E., Shinyashiki, M., Froines, J., Yu, R. C., Fukuto, J. M., and Cho, A. K. (2004). An examination of quinone toxicity using the yeast Saccharomyces cerevisiae model system. *Toxicology* **201,** 185–196.

Rodriguez, C. E., Sobol, Z., and Schiestl, R. H. (2008). 9,10-Phenanthrenequinone induces DNA deletions and forward mutations via oxidative mechanisms in the yeast Saccharomyces cerevisiae. *Toxicol. In Vitro* **22,** 296–300.

Rowlands, M. G., Newbatt, Y. M., Prodromou, C., Pearl, L. H., Workman, P., and Aherne, W. (2004). High-throughput screening assay for inhibitors of heat-shock protein 90 ATPase activity. *Anal. Biochem.* **327,** 176–183.

Shinyashiki, M., Eiguren-Fernandez, A., Schmitz, D. A., Di Stefano, E., Li, N., Linak, W. P., Cho, S. H., Froines, J. R., and Cho, A. K. (2009). Electrophilic and redox properties of diesel exhaust particles. *Environ. Res.* **109,** 239–244.

Smart, D. J., Halicka, H. D., Schmuck, G., Traganos, F., Darzynkiewicz, Z., and Williams, G. M. (2008). Assessment of DNA double-strand breaks and gammaH2AX induced by the topoisomerase II poisons etoposide and mitoxantrone. *Mutat. Res.* **641,** 43–47.

Srinivasan, A., Robertson, L. W., and Ludewig, G. (2002). Sulfhydryl binding and topoisomerase inhibition by PCB metabolites. *Chem. Res. Toxicol.* **15,** 497–505.

Sumi, D., and Kumagai, Y. (2007). Chemical biology of 1,2-naphthoquinone, a novel air pollutant that affects signal transduction pathways. *Yakugaku Zasshi* **127,** 1949–1956.

van Agen, B., Maas, L. M., Zwingmann, I. H., Van Schooten, F. J., and Kleinjans, J. C. (1997). B[a]P-DNA adduct formation and induction of human epithelial lung cell transformation. *Environ. Mol. Mutagen.* **30,** 287–292.

Verma, R. P. (2006). Anti-cancer activities of 1,4-naphthoquinones: A QSAR study. *Anticancer Agents Med. Chem.* **6,** 489–499.

Wei, H., Ruthenburg, A. J., Bechis, S. K., and Verdine, G. L. (2005). Nucleotide-dependent domain movement in the ATPase domain of a human type IIA DNA topoisomerase. *J. Biol. Chem.* **280,** 37041–37047.

Willmore, E., Frank, A. J., Padget, K., Tilby, M. J., and Austin, C. A. (1998). Etoposide targets topoisomerase IIalpha and IIbeta in leukemic cells: isoform-specific cleavable complexes visualized and quantified in situ by a novel immunofluorescence technique. *Mol. Pharmacol.* **54,** 78–85.

Downloaded from https://academic.oup.com/toxsci/article/126/2/372/1687885 by Ahmedabad University user on 01 May 2025